UNIVERSITY OF COPENHAGEN

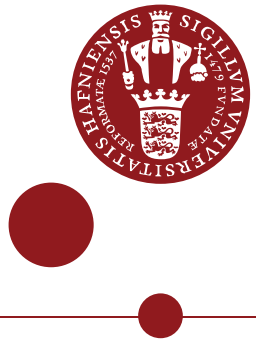

MSc in Physics

Hitting rock bottom

How the Earth system resists cooling and/or lowering atmospheric CO_2 concentrations during the glacial periods

Marta Agnieszka Mrozowska

Supervised by Markus Jochum

Handed in: 23rd of August, 2021

Marta Agnieszka Mrozowska
Hitting rock bottom: How the Earth system resists cooling and/or lowering atmospheric CO_2 concentrations during the glacial periods
MSc in Physics
E-mail: gsl536@alumni.ku.dk
Handed in: 23/08/2021
Defended: 02/09/2021
Supervisor: Markus Jochum

University of Copenhagen
Faculty of Science
Niels Bohr Institute
Blegdamsvej 17
2100 Copenhagen

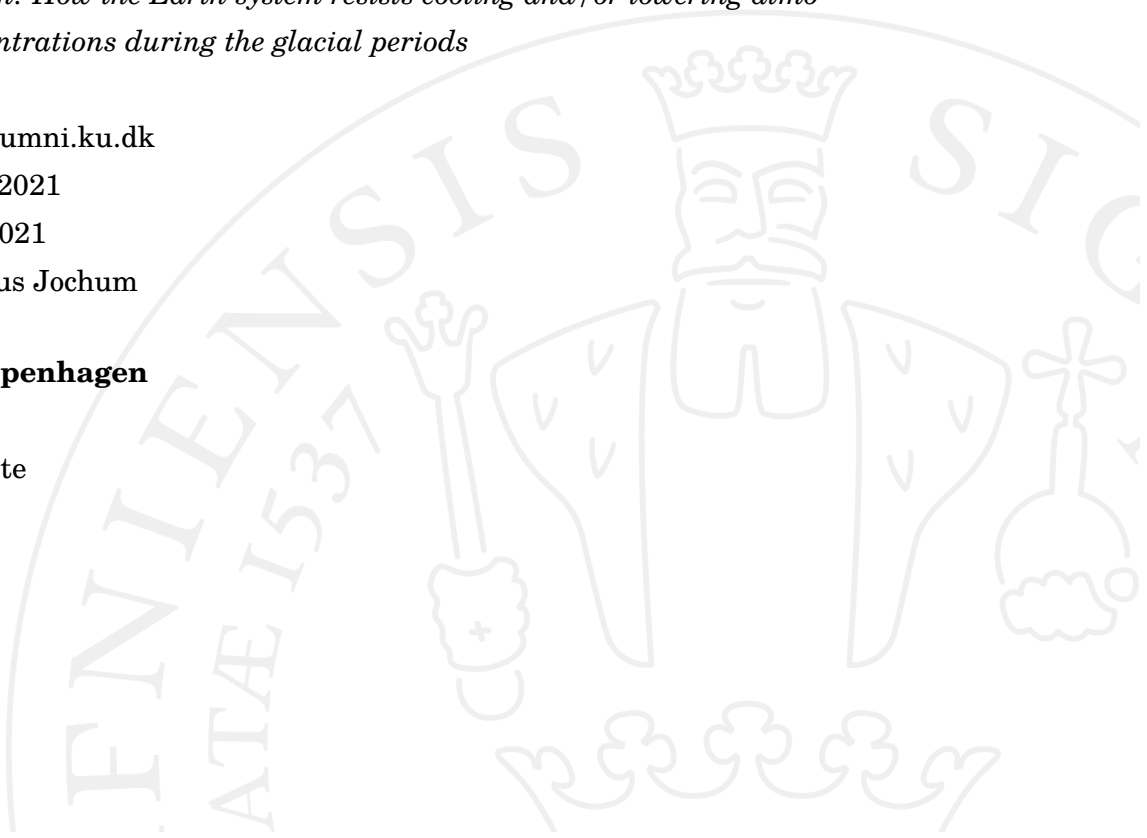

Marta A. Mrozowska

Hitting rock bottom

HOW THE EARTH SYSTEM RESISTS COOLING AND/OR LOWERING ATMOSPHERIC CO_2 CONCENTRATIONS DURING THE GLACIAL PERIODS

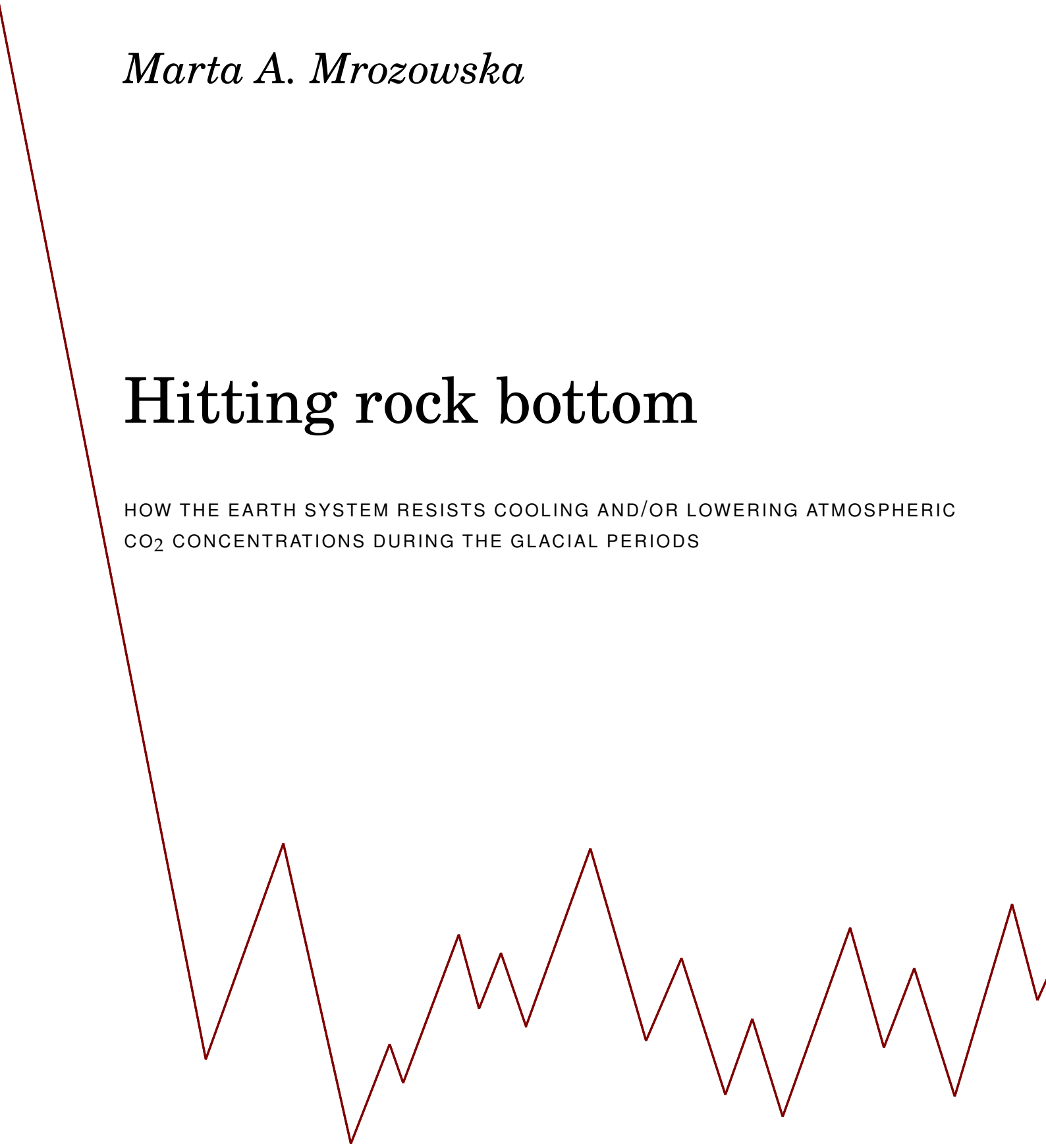

Supervised by Markus Jochum

ABSTRACT

Over the past 800 thousand years, the Earth system has gone through a series of glacial-interglacial cycles. The glacial paleo-climatological records show a consistent lower limit for both the atmospheric CO_2 levels and the temperature. This motivates a hypothesis that a potential negative feedback effect is in place which keeps the Earth system above these limits. In this work, five of the negative feedback hypotheses are presented, described in detail and tested using output from fully coupled Community Earth System Model. The modeled glacial conditions match the observed Last Glacial Maximum CO_2 levels and temperatures. The output analysis reveals that the lower CO_2 limit does not exist in the model, but the temperature limit does. Nutrient trapping, found in previous model studies, is also present in the output. The productivity in the global ocean is limited due to high phytoplankton activity in the Southern Ocean, which could be a potential overlooked negative feedback effect.

ACKNOWLEDGEMENTS

I would like to thank my supervisor, prof. Markus Jochum, for his guidance in this project. I also owe thanks to Roman Nuterman, who has provided help with any technical difficulties I have encountered. The output analyzed in this thesis has been simulated by TeamOcean, the oceanography group at the Niels Bohr Institute, and without it, the project could not exist. Finally, I thank my parents and my partner, Jonas Søndermølle, for continuous moral support throughout the writing process.

Contents

List of Abbreviations

AABW	Antarctic Bottom Water
AAIW	Antarctic Intermediate Water
ACC	Antarctic Circumpolar Current
AMOC	Atlantic Meridional Overturning Circulation
BGC	Biogeochemistry component
CDW	Circumpolar Deep Water
CESM1	Community Earth System Model version 1.0
D-O	Dansgaard-Oeschger
DIC	Dissolved inorganic carbon
DOM	Dissolved organic matter
G&E	*Galbraith and Eggleston* [2017]
GPP	Gross primary production
HNLC	High-nutrient low-chlorophyll
LGM	Last Glacial Maximum
MOC	Meridional Overturning Circulation
MPT	Mid-Pleistocene Transition
NADW	North Atlantic Deep Water
NH	Northern Hemisphere
NPP	Net primary production
pCO_2	Partial pressure CO_2
POC	Particulate organic carbon
SAT	Surface air temperature
SH	Southern Hemisphere
SO	Southern Ocean
SOMOC	Southern Ocean Meridional Overturning Circulation
SST	Sea surface temperature

List of Figures

List of Tables

"The poet decided to stop writing short poems, resolving instead to devote himself to creating an epic novel. 'In my new work,' he said, 'I want to describe our entire society, our country, and our soul.' Not to be outdone, Milankovitch replied: 'I feel attracted by infinity. I want to do more than you. I want to grasp the entire universe and spread light into its farthest corners.' After sealing their resolutions with another bottle of wine, the two friends parted happily. The years to come would test the strength of their resolve."

- "Ice Ages", Imbrie and Imbrie

Introduction

The glacial-interglacial cycles have been a point of interest in the scientific community for decades. The main reason for this is the correlation between global mean temperature and carbon dioxide levels in the atmosphere. The radiative forcing due to CO_2 is of interest, as it is also a by-product of many anthropogenic industries developed in the past century. The glacial cycles, especially the emergence of the Earth system from the last glaciation, offer a good opportunity to tune our climate models in hopes of predicting future weather scenarios under increased atmospheric CO_2 levels. However, the details of the correlation between the greenhouse gas concentrations and temperature remain uncertain due to the complex nature of the system. New ideas of tackling the problem emerge regularly, and one recent proposal is to look at the lower limit in CO_2 and temperature records over the past 800 thousand years.

The Earth system appears to resist cooling and lowering atmospheric carbon dioxide concentrations at certain thresholds, which offers a new perspective on the problem: a possibility of a negative feedback effect. This idea is put forward by *Galbraith and Eggleston* [2017][1], who outline four feedback pathways as an attempt to further our understanding of the relationship between CO_2 and temperature. In this study, I attempt to understand, describe and test these feedback pathways.

[1] In this report, I will mostly be referring to this publication as G&E.

The thesis is structured as follows: the second chapter, *Facts and intuition*, is a guide for all topics in physics, biology, paleoclimatology and chemistry necessary to understand the basis in reasoning for the proposed negative feedback effects. The third chapter, *Digital twin of Earth*, describes the climate model which is used to test the negative feedbacks. Next, in *Model realm*, I present the relevant results from the model runs. In *Connecting the dots*, I discuss the results in the context of the negative feed-

backs. Finally, the chapter *Light at the end of the tunnel* sums the entire endeavour up[2].

[2] (And it does turn out to be quite the endeavour.)

This work, in essence, provides a good overlook of the challenges researchers face when dealing with the CO_2 and temperature correlation problem. It seems much more trivial than it is in reality, especially considering that we all have learned about the greenhouse effect in the high school physics class. Without further ado, I invite you to explore this problem as I have done for the past year.

Facts and intuition

We start here on Earth, where you, dear reader, are likely also situated yourself. The Earth as we know it is trees, green grasses, densely populated cities, open countryside, plentiful jungles, dusty cliffs, blue seas, summer rains - it's what we call home. The Earth as we will discuss in the following pages has to be seen in a wider perspective than that of a single human being. And here lies the challenge, which you will surely soon notice by yourself - this complex system that we know from our everyday lives does not become any less complex in the bigger picture. Nevertheless, we attempt to describe and understand it, because it is our home and - so far - we have yet to get another one. We start this journey on Earth, but not the Earth as we know it - instead, we will venture back some 20,000 years ago, when the most recent glacial was at its peak: a point in time termed the Last Glacial Maximum, or simply the LGM.

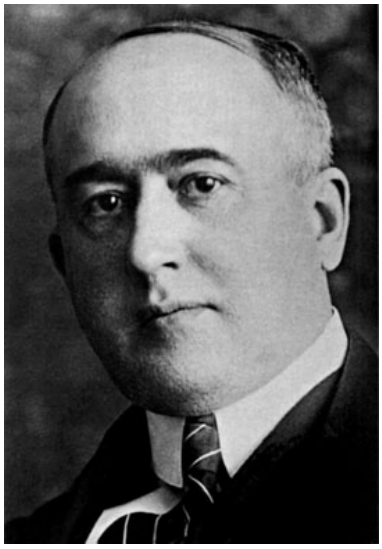

Figure 1: Milutin Milankovitch (28 May 1879 – 12 December 1958) was a Serbian scientist with a wide expertise stretching from mathematics, through astronomy and climate, to engineering. His work cemented the understanding of long term climate cycles, tying in the Earth's orbital obliquity, eccentricity and precession to the variability of ice volume and temperature in the paleoclimatological records.

Last Glacial Maximum

One of the fundamental properties of the Earth system is its variability. From the familiar seasonal climate changes, to vast differences in the environmental structure across geologic epochs, the state of the Earth has always been changing. Due to the nature of the external and internal forcings, the changes are often periodic: simplest and most well known environmental cycles on our planet are the diurnal and annual cycles, but oscillations in climate state occur on longer timescales as well.

The paleo-climatological proxy records are able to take us back to Earth states 500 million years before present, a small fraction of its 4.5 billion year lifetime [*Beer*, 2001]. This discussion, however, doesn't take us back further than 800,000 years before the

current day, at the end of the Mid-Pleistocene Transition (MPT). Since the MPT, the Earth system has been oscillating between glacial and interglacial states with a period ranging from 80,000 to 120,000 years and a characteristic asymmetry.

These transitions have been subject to extensive work done by climate scientists for two main reasons:

1. The period of the oscillations, cited as roughly 100,000 years, does not match any of the significant[3] orbital forcing cycles;

2. The oscillations in temperature and ice volume correlate with atmospheric carbon dioxide concentrations and dust fluxes [e.g. *Peacock et al.*, 2006].

While most agree that the climate transitions before the MPT can be explained by variations in the obliquity angle of the Earth's axis, the past 800 kyr remain a mystery in climate science [e.g. *Chalk et al.*, 2017]. Knowing with certainty what forces these oscillations would provide valuable information about the inner feedback mechanisms in the system and their relative relevance.

Since the MPT, the Earth reached the glacial state eight times, and the most recent of those is also the one we know the most about: the LGM. There are few key features of the glacial Earth:

- During the LGM, the atmospheric partial pressure of CO_2[4] (pCO_2) was at around 190 ppm, compared to the pre-industrial 280 ppm [*Schmitt et al.*, 2012];

- The drop in global average sea surface temperature (SST) amounted to 4-5°C [*Peacock et al.*, 2006];

- The terrestrial biosphere contained about 500 Pg[5] less carbon than in the pre-industrial era, which is estimated to have caused a 15 ppm increase in pCO_2 [*Hoogakker et al.*, 2016];

- Towards the end of the transition into glacial conditions, atmospheric dust depositions were enhanced [*Peacock et al.*, 2006];

- The sea level was 120 m lower than in the pre-industrial era [*Denton et al.*, 2010];

- The meridional overturning circulation (MOC) cell in the Northern Atlantic was shallower [*Lynch-Stieglitz et al.*, 2007].

[3] The Fourier analysis of the geological records reveals 3 oscillation periods for the Earth system: 23, 41 and 100 kyr [*Imbrie et al.*, 1992]. The periods of astronomical parameters were given by Milankovitch as 21 kyr for precession, 40 kyr for obliquity and 92 kyr for eccentricity of the Earth's orbit [*Berger*, 2021]. While the latter is close in length to the desired 100 kyr cycle, it has been showed that the Earth's eccentricity changes result in a significantly weaker insolation variations compared to the obliquity and precession forcings, too weak to explain the strong climate variability after the MPT [*Abe-Ouchi et al.*, 2013]. In fact, this problem has an official name: *The 100,000 year problem* and is a recurring hot topic in the climate sciences [*Raymo and Nisancioglu*, 2003].

[4] I will sometimes refer to pCO_2 as atmospheric CO_2 level.

[5] PgC is a widely used unit for carbon inventories, and it stands for petagram carbon, 10^{15}g carbon. Roughly estimated, 1 PgC $\approx$ 0.5 ppm. The estimation in land carbon loss to pCO_2 increase here contains additional calculations.

These are the facts on which most experts in the field agree on. However, there are still many features of the glacials that remain up for discussion: whether the meridional overturning circulation was weaker [*Du et al.*, 2020], the marine biological pump contribution [*Kohfeld et al.*, 2005] and the effectivity of iron fertilization [*Sarmiento and Gruber*, 2006], to name a few. Proxy data for these properties are sparse, therefore climate scientists have turned to other means in hopes of finding new leads.

E. D. Galbraith and S. Eggleston have turned to statistics, and in their paper *"A lower limit to atmospheric CO_2 concentrations over the past 800,000 years"* [*Galbraith and Eggleston*, 2017] have explored in depth a particularly interesting feature of the glacials: the Earth's atmospheric pCO_2 stays above (190 $\pm$ 7) ppm throughout the entire period. In fact, even in the farther-reaching geological records, the CO_2 levels never reached values below that. Additionally, the deuterium (δD) record, a proxy for atmospheric temperature, shows a similar pattern: the values almost never fall below (-440 $\pm$ 5) ‰ (see both records in fig. 2). This has lead the scientists to hypothesise that a negative feedback effect might be in place, which keeps the pCO_2 and/or global temperature from dropping any lower.

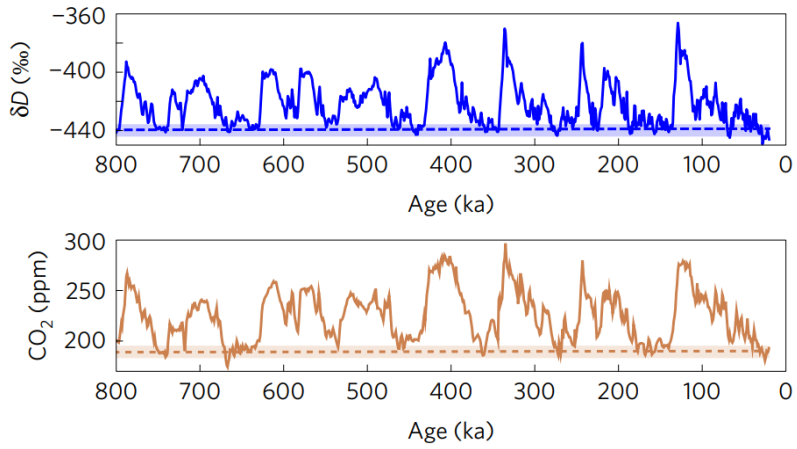

Figure 2: The glacial cycles showing in δD and CO_2 records. The top plot shows the EPICA Dome C ice-core deuterium record, and the bottom plot is a compilation of atmospheric CO_2 records from various ice cores. Source: *Galbraith and Eggleston* [2017].

The following work attempts to describe, explain and test these negative feedbacks within the realm of a modern fully-coupled Earth model. Due to the complexity of the Earth system, we will briefly discuss the relevant topics before getting to the possible feedback pathways outlined by G&E. Since CO_2 is one of the two main players in the story, it seems suitable to begin with...

Carbon cycle

[6] (to humans)

Carbon is one of the most significant[6] elements existing in the universe, due to its chemical structure with four valence electrons relatively close to the nucleus, making it eager to react with other elements. It is one of the fundamental building blocks in organic chemistry, but also found in many familiar inorganic compounds, such as limestone. The carbon cycle is one of the most prominent on Earth, about as important as the hydrological cycle, but far more complex. Its intricacy is the reason why paleo-climatologists are still unsure of the exact processes which governed the atmospheric CO_2 oscillations over the lifetime of the Earth. In this section, we will look closer at the carbon cycle and why we should bother looking for the answer to G&E's lower limit problem.

The reservoirs of carbon existing on Earth include: the atmosphere, the terrestrial biosphere, the ocean, and the inert pools. Figure 3 shows the subdivisions of these reservoirs, their carbon storage abundances and illustrates the fluxes between them.

In the atmosphere, carbon exists primarily either as CO_2 or as CH_4, the latter in lower concentrations. The preindustrial abundance of carbon in the atmosphere is estimated to be 589 PgC. The emissions caused by the industrial revolution are estimated to amount to (240 ± 10) PgC in the present day[7]. In this study, we will compare the LGM carbon inventories to the ones from the pre-industrial era, hence in the following discussion, the contributions from the industrial period will be omitted. The terrestrial biosphere uptakes carbon from the atmosphere in the form of CO_2 at the rate of about 109 PgC/yr and out of that, stores between 450 and 650 PgC. The rest is respired back to the atmosphere or burnt, giving a total net flux of 1.7 PgC/yr from the atmosphere into the terrestrial biosphere. Soils store 1500-2400 PgC, and return it to the atmosphere through microbial respiration and decomposition.

[7] Present day refers to 2013; the values for the carbon fluxes and reservoirs in this section are all sourced from *Ciais et al.* [2013], a chapter in the 2013 IPCC report, as well as discussion in *Goosse* [2015].

Small fluxes of carbon from rock weathering and vegetation enter the ocean through river runoff, and an even smaller fraction gets buried in the sediment of the river bed. The vast majority of the carbon which ends up in the ocean originates from the gas exchange between the surface waters and the atmosphere. Surface ocean stores about 900 PgC, while the abyss and intermediate

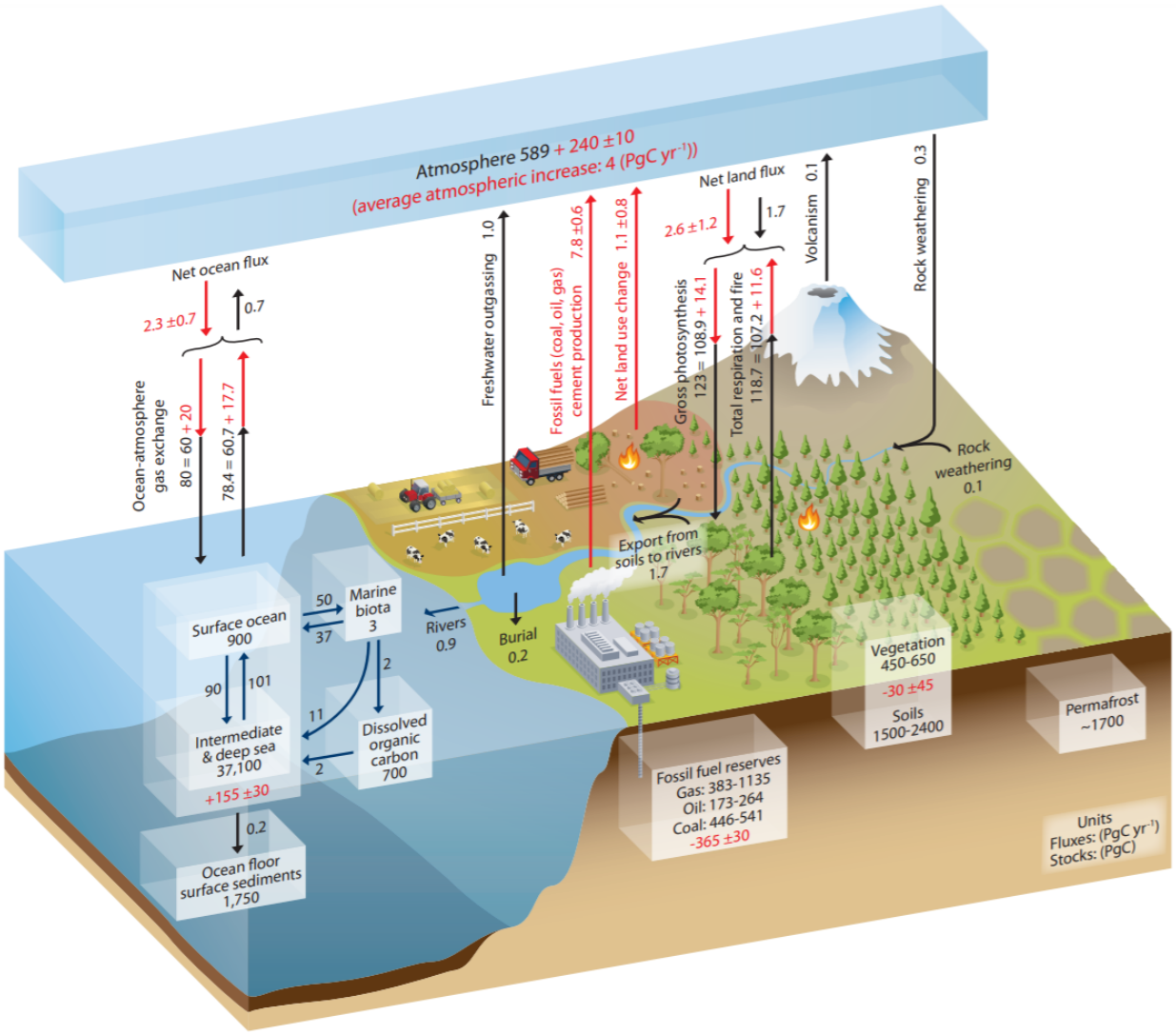

Figure 3: The carbon cycle schematic from *Ciais et al.* [2013]. Fluxes are showed in red with units PgC/yr, and stocks (black) have units of PgC.

waters contain 37100 PgC, amounting to the total of 38000 PgC in the marine inventory.

The sea takes up CO_2 in its aqueous form, which quickly reacts with water, forming HCO_3^-, or bicarbonate ions. This reaction produces H^+ ions, hence increases the acidity of the ocean. The bicarbonate ions can decay into hydrogen and carbonate ions (CO_3^{2-}) and the fraction of the inorganic carbon in the sea which becomes one of the three existing forms is distributed according to the ocean's acidity. In the current state, the abundance of bicarbonate in the ocean waters is at about 90%, with 9.6% of carbonate ions and less than a percentage of aqueous pCO_2. The sum of the three species of carbon are commonly called DIC, which stands for dissolved inorganic carbon. The difference be-

tween the partial pressures of CO_2 at the ocean-atmosphere interface determine the direction of the DIC flux in the region. The CO_2 in the atmosphere is well mixed, with the only major variance coming from the land mass difference between the hemispheres, and seasonal variation due to changes in vegetation. The ocean is inviscid, which means it largely preserves the water mass properties when not in contact with the atmosphere. Therefore, the regional differences of partial pressures of CO_2 in the surface ocean waters are more amplified than those in the atmosphere, and it is the ocean currents which govern the regions of DIC outgassing in the physical realm.

To our disadvantage, reality is not purely physical, as another big player in the marine carbon cycle is of the organic origin. Indeed, the ocean, just like the terrestrial biosphere, has vast ecosystems of its own. These actively respire carbon in the form of CO_2, store it, and export it into the abyss, where it can stay for hundreds of years before getting recirculated into the surface again. Alternatively, the abyssal carbon gets slowly incorporated into the mantle through subduction. The inert sediments at the ocean floor store estimated 1750 PgC. The remaining inert pools of carbon are the fossil fuel reserves, which amount to between 600 and 2000 PgC, permafrost at around 1700 PgC, and the Earth's crust at estimated $50 \cdot 10^6$ PgC. These pools are considered inert, because the carbon exchange with the other reservoirs happens on the timescales of millions of years, through volcanic eruptions, major climate changes and rock formation.

Marine carbon

The abyss is a relatively large carbon storage, and due to the vast area where air-sea gas exchange occurs on Earth, the marine carbon cycle is key to understanding the correlation of atmospheric CO_2 and temperature over the geological period. The concept of oceanic pumps has been developed, which categorizes the sources of DIC in the sea and thereby estimates the relative influence of the various processes involved in exchanging carbon between it and other reservoirs. These are: the solubility pump, governed by physical processes and chemistry, and the biological pump. The solubility pump controls the marine inventory of preformed

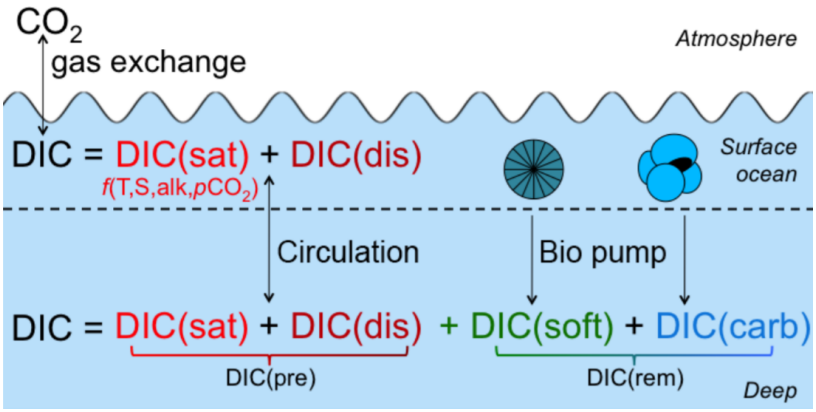

Figure 4: The categorization of DIC based on its source in the ocean adapted from *Eggleston and Galbraith* [2018].

DIC (DIC_{pre}): the carbon which does not get used for respiration at the top of the water column. The remaining DIC content, controlled by the biological pump, is termed as the remineralized DIC (DIC_{rem}). *Eggleston and Galbraith* [2018] expand this concept, creating sub-groups for each of the DIC components (see fig. 4 for the visual breakdown of these components).

As mentioned in the previous section, the relative ratio of the three species of DIC existing in the ocean is dependent on physical properties of the sea water. Unsurprisingly, so is the DIC content in its entirety[8]. Colder waters can hold higher amount of DIC in them, which has both spacial and temporal consequences on the carbon cycle. In order to explain those, we need the concept of disequilibrium DIC, or DIC_{dis}[9]. The amount of preformed carbon in the surface waters would be equal to the saturated carbon, DIC_{sat}, if the atmosphere and the sea were in equilibrium in terms of CO_2 exchange. However, the timescale of reaching such equilibrium is about 10 months, while ocean waters are constantly in motion driven by surface winds and deep water formation. Therefore, the difference between the two quantities exists, and this value is termed the disequilibrium DIC: $DIC_{dis} = DIC_{pre} - DIC_{sat}$. DIC changes through time as the oceanic waters oscillate in temperature when the Earth cools or warms. Additionally, DIC gets sequestered from the atmosphere when the cool waters in the polar regions sink into the abyss as a part of the overturning circulation. Temperature, salinity, sea ice and surface winds all influence the strength of the water flow, thereby altering the timescales at which CO_2 exchange can occur, the effect of which is quantified by DIC_{dis}.

[8] The summary of the marine carbonate chemistry in this section is based on a more detailed description from *Williams and Follows* [2011].

[9] In practice, DIC_{dis} simply means the DIC which ends up in the ocean due to the disequilibrium effect. However, there is no way of distinguishing DIC_{dis} from the rest of the DIC concentration in the ocean by observation. The distinction is only an abstract quantity which helps to understand the marine carbon distribution.

The biological pump[10] refers to the cycling of carbon in the form of organic material between the surface waters and the abyss, and divides into soft-tissue and carbonate pumps. The soft-tissue pump is driven by phytoplankton activity. Marine phytoplankton use photosynthesis to sustain themselves, which requires light energy, CO_2, and nutrients such as nitrate and phosphate. In regions of upwelling, nutrient-rich bottom waters get brought up to the surface, where they are accessible to use within the euphotic zone[11]. In the open ocean, some of the most significant soft-tissue pump activity is in regions termed high-nutrient low-chlorophyll (HNLC), which is fairly self-explanatory: in these regions, the abundance of phytoplankton is low, despite high access to nutrients. One of the most prominent of these is the Southern Ocean (SO). The HNLC regions are characterized by one or more limiting factors for phytoplankton growth, which make them unable to fully deplete all the available nutrients. For example, in the SO, the photosynthesis is strongly limited by light and iron. This also means that these regions are sensitive to changes in these limiting factors: in the case of the SO, if provided with more sunlight or iron, the phytoplankton growth is stimulated, which is usually associated with higher rates of CO_2 uptake. Some of the CO_2 is respired back into the atmosphere, but some of it gets taken down the water column with particulate organic carbon (POC) rain and remineralized in the intermediate and abyssal waters into DIC_{soft}. The carbonate pump refers to the cycling of calcium carbonate ($CaCO_3$) through shell formation in living creatures. A particular type of phytoplankton called *Coccolithophores*, for example, use calcium carbonate to make its exoskeleton, which makes them efficient at burying surface carbon, categorized as DIC_{carb}[12].

The fate of the carbon taken up by the soft-tissue pump has been discussed and researched for decades. It is important to make a distinction between export production and sequestration: export flux is the process by which the CO_2 is taken up from the atmosphere and transported below the euphotic zone by sinking particles. A good measure of the export flux is the POC concentration below the top layer of the water column. However, the exported carbon can still be recycled and respired back into the atmosphere through bacterial activity [*Sarmiento and Gruber*,

[10] *Sarmiento and Gruber* [2006] provide an excellent discussion on the biological pump and the global nutrient distributions.

[11] The zone penetrated by visible light, about 100 to 150 meters at the top of the water column.

[12] The special feature of the carbonate pump is that through the chemical reaction $CaCO_3 \rightleftharpoons CO_3^{2-} + Ca^{2+}$, it decreases alkalinity in the surface ocean and increases it down the water column, which in turn increases the sea surface pCO_2, countering the uptake due to the calcium carbonate burial.

2006]. Sequestration is the flux of carbon below the depth of 1000 meters in the water column, where it can either slowly dissolve or get deposited in the sediments. Sequestration is the process of interest, as it removes carbon from the atmosphere for a relatively long time: abyssal waters are slow and generally re-surface hundreds of years after they are formed.

Herein lays the controversy of iron fertilization. The idea, which started with the oceanographer John Martin, termed *the Iron Hypothesis* [*Martin*, 1990], suggests that CO_2 can be removed from the atmosphere by stimulating phytoplankton growth in HNLC regions with iron. While it is a promising idea, doubts have risen since it has been proposed. It is difficult to assess experimentally whether the CO_2 uptaken by the biological pump makes it below the region in the water column where it can still be recycled [*Sarmiento and Gruber*, 2006]. There is also the concern that when the iron limitation is lifted in the region, another one might come about and stop the CO_2 uptake. Due to uncertainty about the effects of large localized iron inputs on marine ecosystems, the experimentation with iron fertilization has been limited and the hypothesis remains just that.

The world of phytoplankton is rich and surprising, and a particular group has a great influence on the primary productivity in the ocean: *Trichodesmium*, also called sea sawdust. It is a type of cyanobacteria found in nutrient-rich tropical and subtropical ocean waters, and it is responsible for about half the nitrogen fixing[13] in marine ecosystems [*Bergman et al.*, 2013]. Nitrogen fixation in *Trichodesmium* is unique, as it occurs concurrently with photosynthesis. The genus has been of particular interest in marine biogeochemistry research for this reason.

[13] Nitrogen fixation is a process of taking up the N_2 from the atmosphere and transforming it into ammonium or related compounds, effectively a fertilizer for autotrophs (primary producers, organisms which produce their own food by photosynthesis). Nitrogen fixers in aquatic and land ecosystems are called *diazotrophs*.

Hutchins et al. [2007] set out to compare *Trichodesmium* fixation rates under three different pCO_2 and two temperature conditions. The cultures were tested in 150 ppm, 380 ppm and 750 ppm pCO_2 environments. The study demonstrates the cultures died out at background pCO_2 levels of 150 ppm within days. This motivated another paper, *Hutchins et al.* [2013], with a goal to find the value of pCO_2 at which the cultures can no longer survive for extended periods of time. The experiment shows this value to be 180 ppm.

The consequence of this find is quite profound: if the global

pCO_2 was to fall below 180 ppm, it is possible that the *Trichodesmium* cultures would die out, potentially reducing the nitrogen fixation in marine ecosystems by half. One can only hypothesise the effect this would have on marine life and primary productivity, and this is indeed what G&E propose as a key feature in one of the negative feedback effects they outline.

World's Ocean

The motion of the ocean waters is fundamentally intertwined with the cycling of carbon on many timescales. From the surface ocean gas exchange and biological activity, through nutrient and carbon sequestration into the abyss and resurfacing of bottom waters in upwelling, to mantle subduction on the ocean floor, the importance of oceanography in this problem cannot be understated. In this section, we will briefly take a trip into the Earth's sea[14] and outline the water masses which are most significant in G&E's lower limit problem.

[14] The content of this section is based on the in-depth summary of the global ocean circulation in *Talley* [2013].

Figure 5 shows the global overturning circulation (GOC) flowing out of the Southern Ocean basin into the Atlantic, Pacific and Indian Oceans. It serves as an overview of the flows around Antarctica, but not all of the water masses will be discussed in this section, as not all of them are relevant to the problem. Figure 6 shows a simplified 2D schematic of the Atlantic Meridional Overturning Circulation (AMOC), which is largely the focus in this study.

We start at the North Pole, where sea ice formation and low temperatures cool down and saline up the waters incoming from the Atlantic and Pacific gyres. The significant density increase causes the water mass to sink, forming North Atlantic Deep Water (NADW), which fills the basins of the Atlantic and Pacific Oceans below 1000 m depth. NADW travels across the world to finally upwell in the Southern Hemisphere, where it reaches the Antarctic Circumpolar Current (ACC). This is arguably the most unique space of the World's Ocean, as the Drake's Passage allows for the sea to flow along all longitudes without a land mass blocking the way. This results in the most turbulent of ocean's currents driven by the surface winds of the region, the subpolar Westerlies. South of these, by the coast of Antarctica, the

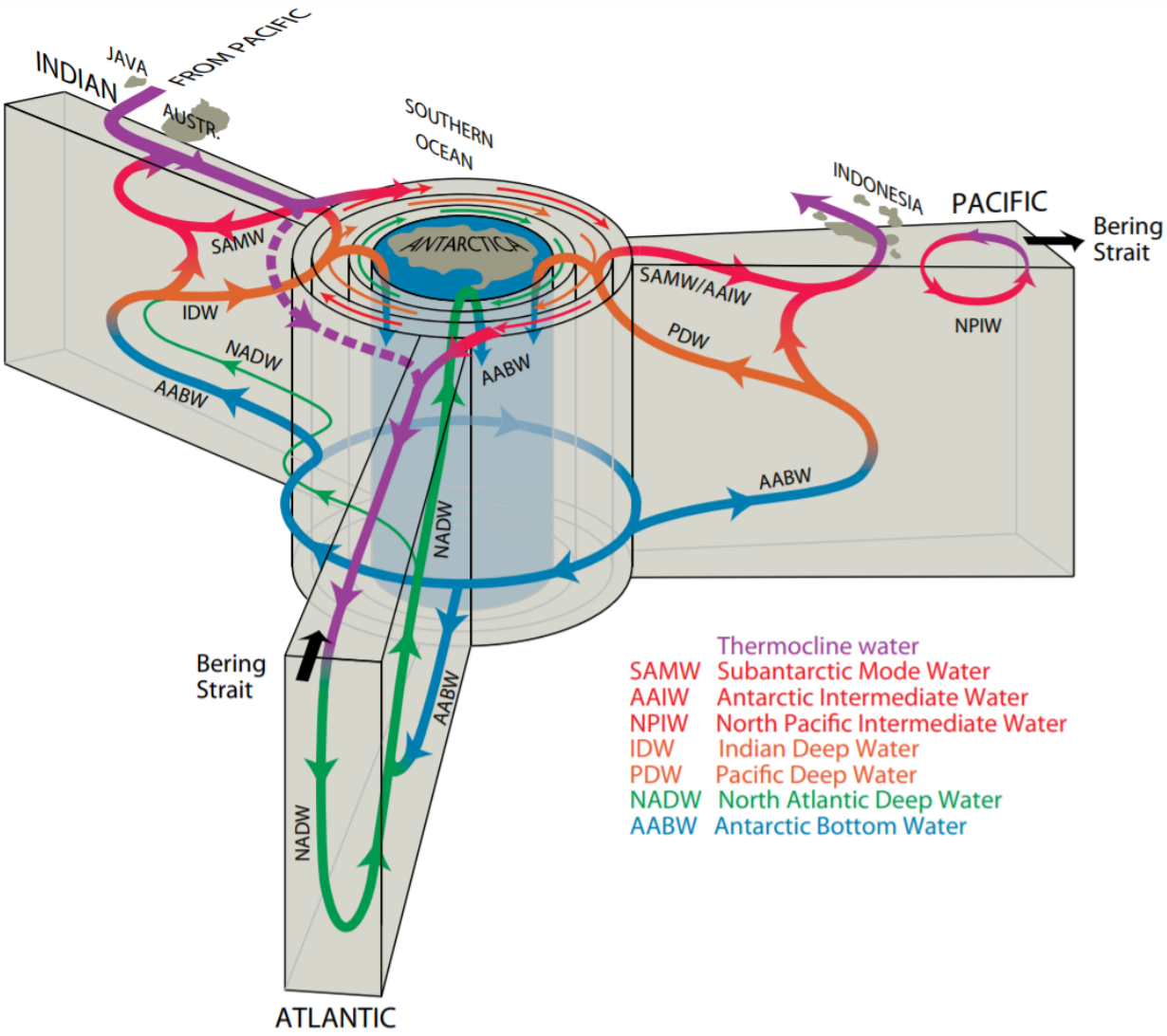

Figure 5: A schematic of overturning circulations around Antarctica splitting into the three ocean basins: Atlantic, Pacific and Indian. Note that AABW supplies the surface and intermediate waters of all three basins, and thereby also the nutrients and the DIC. Source: *Talley* [2013].

Polar Easterlies are directed the opposite way, and the curl of the wind stress on the surface waters induces poleward Ekman transport. North of the ACC, the changing wind stress induces equatorward Ekman transport, which results in a vast region of divergence around Antarctica. Here, the NADW upwells, and splits. The portion of the water mass which continues southward towards Antarctica gets cooled down and becomes more saline due to ice formation, and sinks to form Antarctic Bottom Water, AABW. This water mass is the densest in the world and forms an overturning cell below the NADW, termed the Southern Ocean Meridional Overturning Circulation (SOMOC).

A portion of NADW flows equatorward, losing density due to surface precipitation, and becomes thermocline water. At the

Antarctic Convergence Zone, it encounters significantly warmer Subantarctic Waters, which causes it to sink and transform into Antarctic Intermediate Waters (AAIW), flowing on top of the NADW and underneath Subantarctic Waters. It is transported to all ocean basins with the help of the ACC and can extend as far as 20°N. Underneath the ACC flows the Circumpolar Deep Water (CDW), a mix of NADW, AABW, AAIW, as well as recirculated deep water from the Indian and Pacific Oceans.

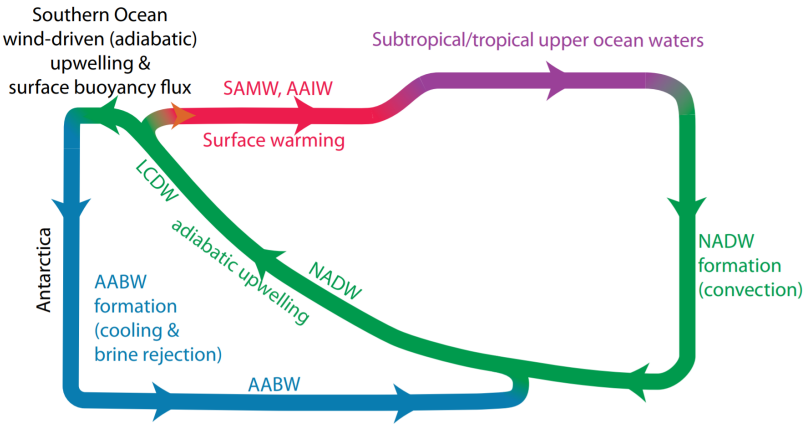

Figure 6: Two-dimensional cross-section schematic of AABW and NADW formations adapthed from *Talley* [2013].

As mentioned in the previous section, the nutrients available to the phytoplankton, as well as DIC, upwell with the abyssal waters. Therefore, NADW and AABW are the most significant in determining the DIC fluxes at the air-sea interface. AABW, due to its proximity to the Antarctic Convergence, is typically oversaturated with DIC. NADW, on the other hand, is formed from the inflow of surface waters into the Arctic, which tend to be depleted from DIC due to biological uptake in the euphotic zone. Despite the biological uptake, the upwelling zones are generally dominated by DIC outgassing due to this high saturation. Conversely, zones of downwelling generally uptake DIC into the ocean.

Ice

The defining factor of glacial periods is the ice cap volume at the poles. Ice has a central role in the climate transitions on Earth for multiple reasons:

- Snow and sea ice albedos are high; this allows for the ice-albedo feedback, where growing ice caps and sea ice cool the Earth, allowing for further ice growth [*Jochum et al.*, 2012];

- Deep water formation occurs at the poles, where the in-flowing waters are cooled down and sink into the abyss; the extent of sea ice influences the strength of the deep water formation, as well as the mean ocean temperature [*Williams and Follows*, 2011];
- Sea ice extent has a potential of limiting phytoplankton growth in the region due to light limitation, as well as suppressing the air-ocean exchange of pCO_2 [e.g. *Stephens and Keeling*, 2000; *Gupta et al.*, 2020];
- Similarly, ice caps cover the fertile ground and limit the extent of the terrestrial biosphere; when the ice caps melt, the carbon stored in permafrost can be again released into the atmosphere [*Ciais et al.*, 2012];

Gupta et al. [2020] simulate a series of experiments with a channel model to quantify the relative importance of the capping and light attenuation effects of sea ice. Capping blocks the air-sea interface, thereby lowering outgassing. In contrast, light attenuation lowers the productivity of the phytoplankton in the region, which reduces the pCO_2 uptake. They find that in their model, the normalized integrated carbon flux F_n is dependent on a factor λ_0, which is defined as:

$$\lambda_0 = \frac{\tau_{res}}{\tau_e + \tau_b},$$

where τ_{res} is the time of the water parcel spent under the ice, τ_b is the time scale of biological exchange, and τ_e is the gas exchange at interface time scale. In other words, they find that the impact of sea ice on the carbon cycle depends on the balance between the three timescales.

Land

Just like marine phytoplankton, plants use photosynthesis to respire and grow. The total amount of carbon exchange with the atmosphere is termed Gross Primary Production (GPP). A fraction of uptaken CO_2 is used for respiration, and the remaining carbon stays in plants and is used for growth of roots, stems and leaves. This fraction of GPP is termed the Net Primary Production, or the NPP [*Gough*, 2011]. The NPP is widely used to assess

the effect of various environmental factors on carbon storage.

The plants uptake CO_2 from the atmosphere in the process of photosynthesis[15]. The photosynthetic carbon assimilation, A, is equal to $g_{CO_2}(C_a - C_i)$, where C_i is the CO_2 concentration inside a leaf, C_a is the background CO_2 concentration, and g_{CO_2} is the conductance of CO_2. By maximizing g_{CO_2}, the plant can maximize A, and therefore uptake more CO_2 from the atmosphere. The conductance of CO_2 can be maximized by having large, open stomata[16], or having large concentrations of photosynthetic enzymes, such as RuBisCO. As with all systems, there are limitations to this: large stomata let out water, which can be a problem for the plant in dry conditions. Likewise, the concentration of the RuBisCO enzyme is limited by the plants' access to nitrogen.

The glacial terrestrial biosphere is estimated to have contained 300 to 700 less PgC than the pre-industrial era, corresponding to about 15 ppm in atmospheric pCO_2 [*Hoogakker et al.*, 2016]. Pollen analysis and model studies show that dry, cold glacial conditions favor grasslands, tundra and deserts over forests. Model studies also show the decline of NPP in the LGM down to 42-48 PgC/yr, however these models slightly overestimate the present day NPP values. The LGM NPP values estimated from isotopic proxies have been cited as (20±10) PgC/yr [*Ciais et al.*, 2012].

[15] The discussion about photosynthesis and the photosynthetic pathways in the following paragraphs is based on *Forseth* [2010].

[16] Stomata are the pores on the bottom of leaves which plants use for CO_2 and water exchange with the atmosphere.

Four feedback pathways

Now that we are more knowledgeable on the intricacies of the Earth climate system, it's time to get back to the problem at hand: what causes the lower limit in the pCO_2 and temperature ice core records? G&E outline four pathways and five different hypotheses for possible negative feedback mechanisms which resist further cooling and/or lowering of pCO_2.[17]

The **(TT)** pathway is the temperature controlled negative feedback which *resists further cooling at low temperatures*. The idea here is that in cold climates, a physical limit is reached which stops the rest of the system from cooling. Such a physical limit might be the freezing temperature of sea water: -2.5°C. The ocean cannot be cooled below this point, which puts a limit on the atmospheric temperature due to air-sea heat exchange. G&E

[17] The hypothetical feedback effect is not supposed to cause deglaciation. Rather, its role is to retain the conditions already in place by resisting processes that lower the temperature and/or the pCO_2 levels.

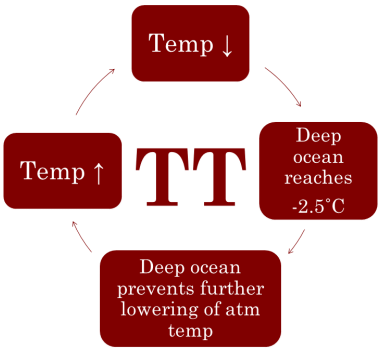

deem this pathway the least plausible, as deep waters only meet the atmosphere at the poles where they are formed, in a relatively small fraction of the ocean's surface area. Moreover, in the models, the temperature keeps falling when pCO_2 is decreased below 180ppm.

The **(CT)** pathway is temperature controlled negative feedback where *the CO_2 impact on temperature is reduced in the cold state*. This means that an effect would be in place which reduces the climate response to radiative forcing from CO_2 as the temperature falls. According to G&E, this pathway is in conflict with the tendency of models to show an increasing sensitivity to radiative forcing as the climate cools [*Manabe and Bryan Jr.*, 1985].

The **(TC)** pathway involves *preventing the lowering of CO_2 as Earth grows very cold*. There is potentially a wide range of physical mechanisms which could cause this. One of the most common theories about the mechanism responsible for the temperature-CO_2 correlation is the ice capping in the SO. The orbital configuration induces a positive albedo feedback which increases the sea ice concentration at the poles. Aside from the ice capping effect, the new climate causes changes in the ocean currents, which both result in increased CO_2 uptake from the atmosphere [*Kohfeld and Chase*, 2017]. This hypothetical pathway assumes there is a limit to this effect, and the growing cold conditions shift the system from uptake to outgassing as temperatures decrease. As a result, CO_2 accumulates in the atmosphere, countering the system cooling through radiative forcing.

The final pathway, **(CC)**, is a CO_2 controlled negative feedback where *the lowering of the ambient pCO_2 causes carbon loss from one of the remaining reservoirs into the atmosphere*. G&E outline two hypotheses that might be at play here: **(CC^a)**, which focuses on ambient pCO_2 limiting global photosynthesis, and **(CC^b)**, where specifically marine primary production is limited.

In **(CC^a)**, the marine and terrestrial ecosystems respond to lower ambient pCO_2 levels with reduced NPP due to limited photosynthesis. NPP is responsible for the long-term carbon storage in plant stems and roots, and its reduction causes CO_2 to be returned into the atmosphere through decomposition.

(CC^b) proposes that at low atmospheric concentrations of CO_2, the colonies of marine diazotrophs die out, significantly

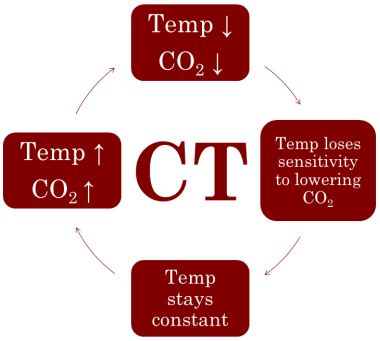

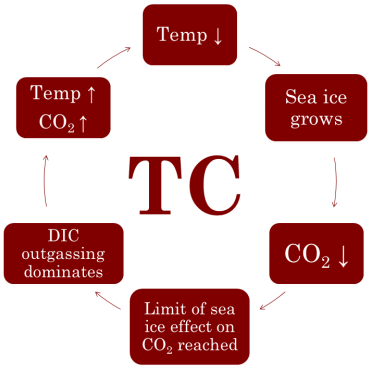

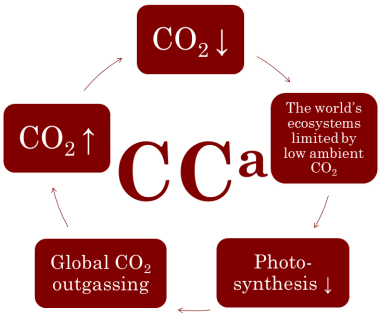

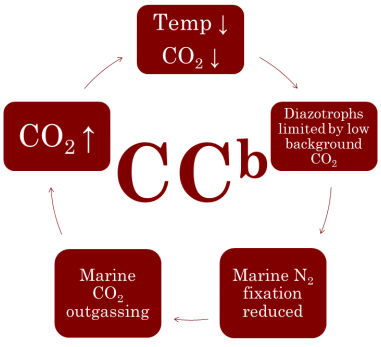

reducing the nitrogen fixation in the sea. This is detrimental to the other phytoplankton species in the ocean, which end up with less available nutrients, resulting in reduced growth and thereby, lower uptake of CO_2 from the atmosphere.

Digital twin of Earth

In this study, we will look at the output of various sensitivity experiments ran in the coarse resolution Community Earth System Model version 1.0 (CESM1) [*Hurrell et al.*, 2013]. The output is provided by TeamOcean at the Niels Bohr Institute, University of Copenhagen and to be published in *Jochum et al.* [submitted]. It simulates the conditions from the LGM and tests the sensitivity of the system to alterations in two variables. In this section, I will describe the output, the relevant model features and the analysis challenges.

The model includes coupled ocean, atmosphere and land components. The ocean model consists of a 116x100 point grid and 60 vertical layers, and the resolution is location-dependent, with highest resolution at the poles and lowest in the equatorial regions. The atmospheric component runs with 3.75° resolution and 26 vertical layers. The choice of coarse resolution is justified by lower cost of computation, while allowing for simulations that can reproduce Dansgaard-Oeschger (D-O) events and LGM conditions [*Vettoretti and Peltier*, 2015]. See *Shields et al.* [2012] for a detailed comparison between this model and ones with more costly, higher resolutions.

Ocean component

The ocean is coupled with sea ice and marine biogeochemistry component (BGC). The details of the BGC implementation can be found in *Moore et al.* [2004] and *Lindsay et al.* [2014]. The ecosystem includes nutrient tracers (nitrate, ammonium, phosphate, dissolved iron, silicate), phytoplankton functional groups (diazotrophs, small phytoplankton and diatoms), zooplankton, dissolved organic matter (DOM) and sinking particle detritus.

Coccolithophores are included implicitly.

Diazotrophs, which are heavily limited by background pCO_2, do not have this limit in the model. The C/N/P elemental ratios are kept fixed within all the functional groups, but are allowed to vary with dissolved organic matter (DOM). Diazotroph C/N/P ratio is set to 329/45/1, in order to reflect high C/P ratios observed in *Trichodesmum* [*Moore et al.*, 2004]. They are also the only functional group which is directly limited by temperature, drastically reducing their growth at 15°C. Their direct contribution to the marine primary production is small, but indirectly they fuel 10% of it by fixing nitrogen. Growth rates at lower temperatures[18] are reduced for all phytoplankton functional groups, and they can be multiplicatively light and nutrient co-limited.

Moore et al. [2004] report that nitrogen fixation is underrepresented in the model. However, when the N-fixation is increased, this leads to depletion of phosphate below observed levels, and the diazotrophs experience strong P-limitation.

[18] Low temperatures also affect the production of $CaCO_3$: below 5°C, $CaCO_{3prod}$ = $CaCO_{3prod}$ (T+2.0)/7.0.

Land component

CESM1 uses the Community Land Model version 4 (CLM4) *Lawrence et al.* [2011], which is an improved version of CLM3.5 [*Lawrence and Chase*, 2007].

The land vegetation is extended with a prognostic carbon-nitrogen (CN) biogeochemical model based on *Thornton et al.* [2002]. This allows for more complex terrestrial interactions. CN computes, among others, leaf and stem area indices, carbon and nitrogen concentrations, and net and gross primary production. In general, leaf loss occurs if one of the 3 following conditions is true:

1. A sustained period of dry soil occurs;
2. A sustained period of cold temperature occurs;
3. Day length is shorter than 6 hours.

If none of these triggers activate, the leaves are allowed to persist all year round.

The maximum rate of carboxylation in the photosynthesis component of the CN model is calculated as a function of a number of conditions, including the leaf C:N ratio and RuBisCO enzyme

activity, which is itself a function of leaf temperature. Therefore, the photosynthesis rate is directly affected by temperatrue, but not limited by background pCO_2. The stomatal conductance in the model is not affected by it either. Decomposition, which is responsible for the flux of plant carbon into the atmosphere, depends on the size of the litter and SOM pools, as well as on soil temperature and moisture.

Output

A range of experimental output will be analyzed in the following pages. Here, each experiment[19] is briefly described.

[19] In the analysis, I make a distinction between an *experiment* and a 100 year steady state *average*. For example, the **LGM** experiment refers to the entire 5000 year long simulation run. The **LGM** average refers to the mean output values from years 3900-4000 in the **LGM** experiment.

PRE: Preindustrial setup based on 1850 CE forcings. Tidal mixing is used as described in *Bryan and Lewis* [1979], and the overflow parameterization *Danabasoglu et al.* [2010] is removed, as the information needed to set up these components is not known for the LGM conditions. The simulation is run for 5000 years.

LGM: Like **PRE**, except orbital forcing is set to parameters from 21 kya, with corresponding ice sheet orography, ocean bathymetry and sea level (120 m lower with corresponding 5.7% smaller ocean volume; the concentrations of tracers are increased accordingly). Land emerging due to changed sea level is assigned the type of its nearest neighbour. Salinity is increased by 1 psu. Just like **PRE**, **LGM** is integrated for 5000 years.

LGMd: Like **LGM**, except after 3000 years vertical diffusivity is doubled. The experiment is run for 4000 years.

LGM5i: Like **LGM**, but after 3000 years aeolian dust fluxes are multiplied by five, resulting in total 6000 year long run.

LGM10i: At year 6000, this experiment branches out of **LGM5i** and the aeolian dust fluxes are increased again, resulting in 10 times higher dust input than in **LGM**. The experiment runs for 4000 years.

The timeseries of pCO_2 and AMOC strength in the experiments can be seen in figures 7 and 8. The runs take one day to simulate 90 model years on 160 cores [*Jochum et al.*, submitted].

Since the model does not include active sediments or inert pools, the main assumption of the **LGM** experiment is that 1480 PgC is removed from the system due to those inventories. The assumption is based on *Ciais et al.* [2012] estimate of inert land carbon pool (400-1000 PgC) and *Cartapanis et al.* [2016] estimate of ocean sediment (200-500 PgC) inventory increases in the last glacial.

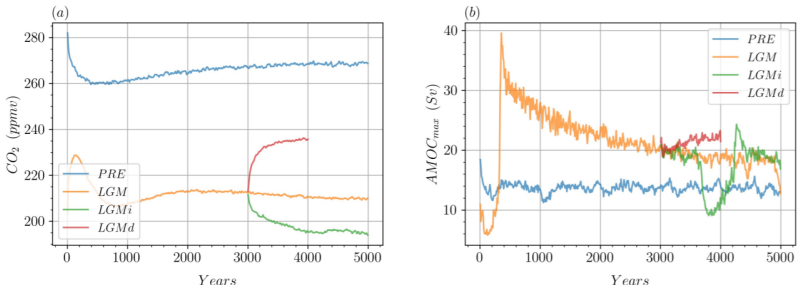

Figure 7: The timeseries of (a) pCO_2 and (b) AMOC strenght in **PRE** (blue), **LGM** (orange), **LGM5i** (green) and **LGMd** (red). Note that on the figure and in *Jochum et al.* [submitted] (where the figure is sourced), **LGM5i** is termed *LGMi*. This is because *Jochum et al.* [submitted] do not use the **LGM10i** run, and therefore do not have to make the distinction between them.

LGM5i and **LGM10i** develop Dansgaard-Oeschger (D-O) events. Since the stadial and interstadial periods are both steady states, this motivates using two time averages in these experiments, rather than one. Table 1 shows the model years used for calculating the time means. The stadial and interstadial periods were chosen based on the AMOC strength. The *zero* states are the means taken during interstadials, except for **LGM0**, since the **LGM** experiment did **not** develop the D-O events. Instead, **LGM0** is used for a more accurate comparison between the **LGM5i** interstadial. When looking at global variable distributions, interstadial states will be used for analysis, as the stadial states introduce some additional processes which make comparisons less straight-forward.

Table 1: The list of time averages used for analysis. The zero states, **LGM5i0** and **LGM10i0**, correspond to the interstadial periods. **LGM0** is used for a better comparison with **LGM5i0**.

Name	Time average [yr]
PRE	3900-4000
LGM	3900-4000
LGM0	3500-3600
LGMd	3900-4000
LGM5i	3900-4000
LGM5i0	3500-3600
LGM10i	9505-9605
LGM10i0	9805-9905

The D-O events show up in the timeseries of numerous variables, which is demonstrated in figure 8 for the **LGM10i** experiment. However, there is a phase shift present in some of the variables. Due to the lead of ocean temperature in the D-O oscillations, the stadial and interstadial values are nearly identical at the chosen 100 year averages. The difference between the last minimum and maximum of the average ocean temperature is about 0.15°C, hence the issue with the lead is not too significant, but worthy to keep in mind.

The presence of the D-O events is reassuring in terms of reproducing the authentic conditions of the climate system, but makes

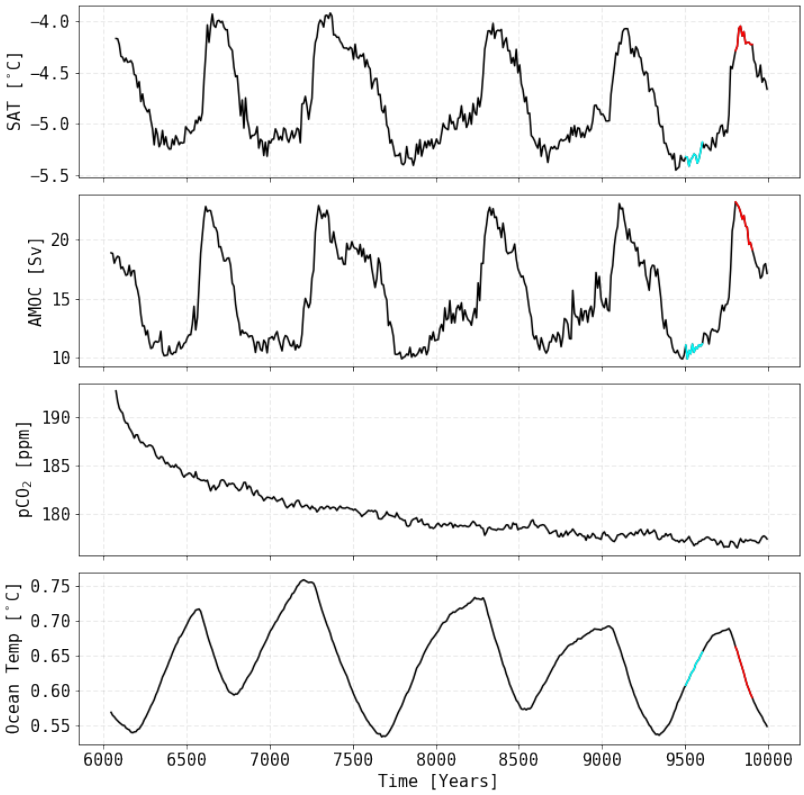

Figure 8: The average surface air temperature (SAT), Atlantic meridional overturning circulation (AMOC) strength, atmospheric pCO_2 and ocean temperature over the integration period of the **LGM10i** experiment. The D-O events are clearly visible in all variables except for pCO_2. The blue period (years 9505 to 9605) corresponds to the 100 year average chosen as the stadial **LGM10i**. The red period of years 9805 to 9905 corresponds to the 100 year average chosen as the interstadial **LGM10i0**.

it difficult to draw conclusions from the steady state simulations. For example, the strength of the overturning circulation is important in the carbon cycle analysis. However, it varies greatly between the stadial and interstadial states in the model output, while the pCO_2 remains effectively unchanged (see AMOC and pCO_2 on fig. 8).

This study will focus on the **LGM10i** experiment for multiple reasons: it is the simulation which is not discussed in *Jochum et al.* [submitted], nor in the master's thesis *Möllney* [2020], which otherwise analyze the same model experiments. Moreover, the **LGM10i** is the only run which ends up at a lower than 190 ppm level of pCO_2.

Model realm

The specifications outlined in *Digital twin of Earth* reveal that there is a limit to which processes are and can be implemented in a fully coupled climate model. In this chapter, we will consider a range of variables from the simulated output in order to assess if there is evidence for or against any of the four hypotheses outlined by G&E.

Temperature and carbon

Temperature and carbon are the focus variables in the negative feedback hypotheses. In this section, I investigate the carbon levels in various reservoirs, and how these levels are affected by temperature and other physical properties of the system.

The pCO_2 only falls below 190 ppm in the **LGM10i** experiment. The minimum and mean levels of pCO_2 for each steady state average are listed in Table 2. Figure 9 shows the mean surface (SAT), sea surface (SST) and ocean temperatures as functions of pCO_2. As expected, the temperature increases with raising atmospheric CO_2. The **LGM5i** stabilizes at temperatures only marginally colder than in **LGM** (within 0.5°C for both the stadial and interstadial comparison), but with a pCO_2 value of about 12 ppm lower. This is consistent with estimation in *Jochum et al.* [submitted] that fivefold increase in iron dust fluxes leads to about 15 ppm decrease in pCO_2. However, the drop in pCO_2 is higher between **LGM5i** and **LGM10i**: the difference between the interstadials amounts to about 22 ppm. Additionally, with such a change in pCO_2, we would expect a greater difference in temperatures between these three experiments.

The plot of mean ocean temperature with respect to atmospheric pCO_2 reveals a clear plateau in their correlation. Al-

Table 2: Minimum and average pCO_2 values recorded in each set of the model output.

	min pCO_2 [ppm]	mean pCO_2 [ppm]
PRE	267.9	269.1
LGMd	235.1	236.2
LGM0	210.9	211.7
LGM	210.1	210.9
LGM5i0	198.2	199.2
LGM5i	195.0	196.0
LGM10i	176.4	177.1
LGM10i0	176.5	177.1

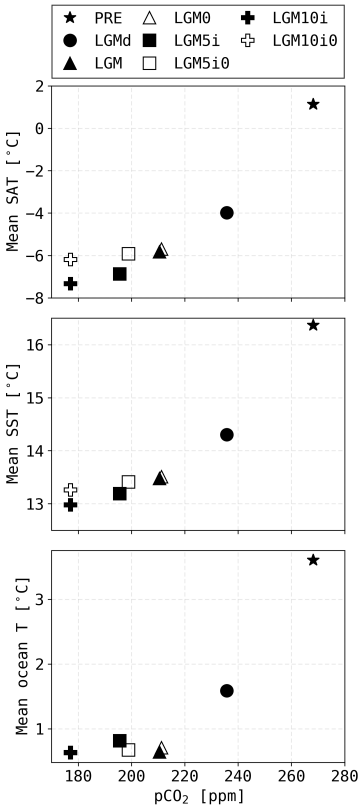

Figure 9: Mean surface air temperature (top), mean sea surface temperature (middle) and mean ocean temperature (bottom) as functions of atmospheric pCO_2.

though pCO_2 drops some 35 ppm between **LGM0** and **LGM10i0**, the six steady states reach equilibrium mean ocean temperatures within the range of 0.6 to 0.8°C[20].

These results show that *the model runs do not exhibit the lower limit for pCO_2, but such a limit does exist for temperature*, which is clearest seen in the ocean. Sea water resists further cooling against the change of radiative forcing caused by decreased pCO_2. A zonal average of the ocean temperature in figure 10 reveals that the distribution of temperature stays nearly identical in **LGM0**, **LGM5i0** and **LGM10i0**, except for the two points of deep water formation: AABW is getting colder and NADW is getting warmer.

[20] Recall that due to the marine lead in the D-O oscillations, **LGM10i** value for average stadial ocean temperature does not reflect the lowest temperature of the **LGM10i** ocean (about 0.55°C).

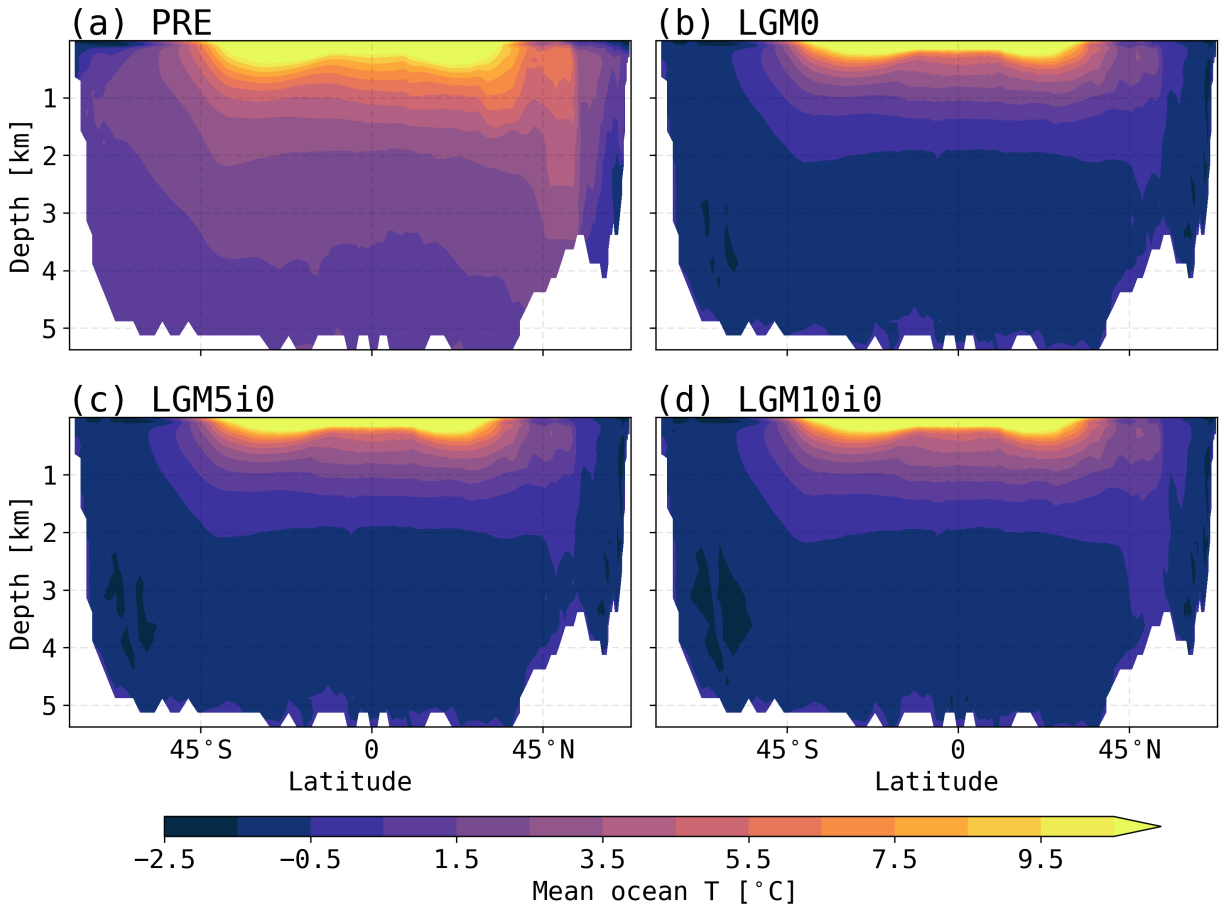

Figure 10: Zonal mean sea temperature in (a) **PRE**, (b) **LGM0**, (c) **LGM5i0** and (d) **LGM10i0**. The lower limit on the colorbar, -2.5°C, is the freezing temperature of sea water.

Figure 11 reveals that SAT also contains the localized warming signal seen in the ocean temperatures. The physical conditions in the **LGM** experiment result in steeper temperature gradient between the poles and the tropics compared to **PRE**. The tem-

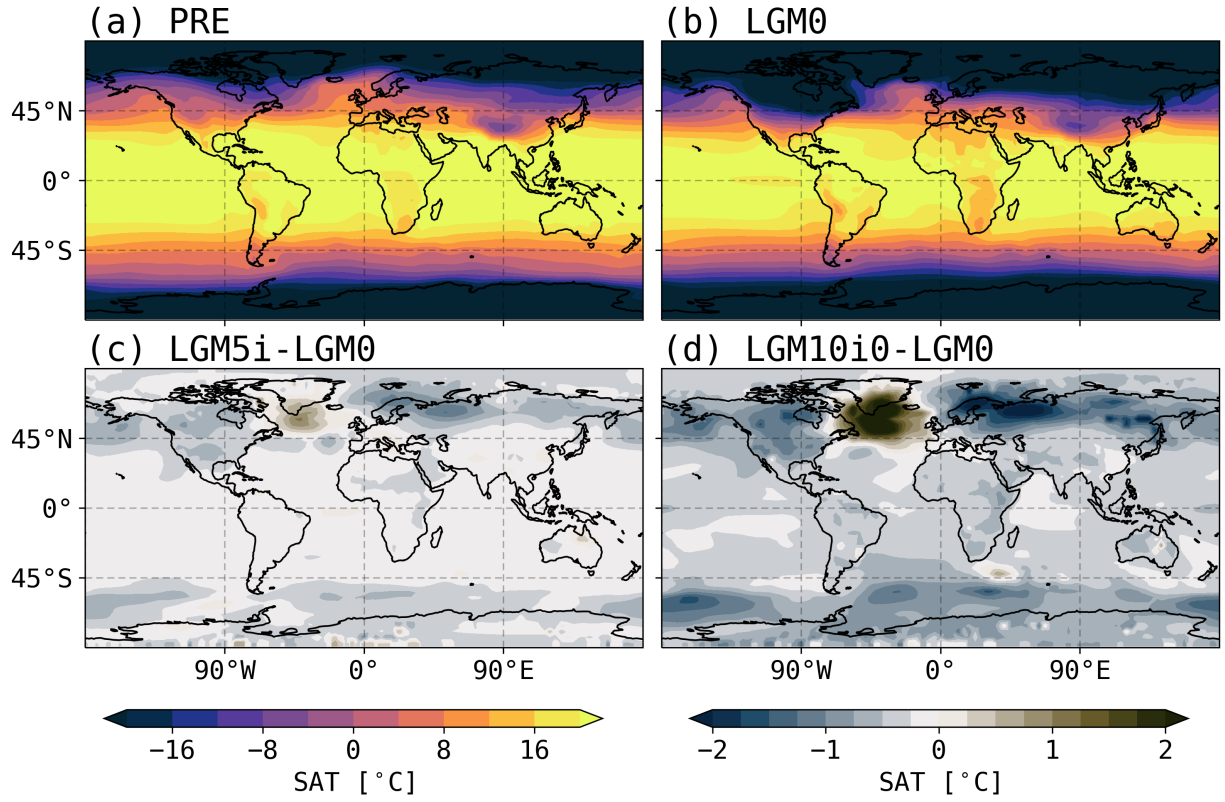

Figure 11: Global surface air temperature (SAT) distribution in (a) **PRE**, (b) **LGM0**, (c) **LGM5i0-LGM0** and (d) **LGM10i0-LGM0**. The maximum warming from **LGM0** to **LGM10i0** in the hot pocket in Northern Atlantic is equal to 3.05°C.

perature differences between **LGM0** and the interstadials with enhanced iron fluxes are lower in magnitude. An interesting feature is the hot pocket above the Northern Atlantic. In **LGM5i0**, the warming in the region is of only 1°C at maximum, but in **LGM10i0**, the SAT difference compared to **LGM0** reaches 3°C.

It appears that these warm regions in the Northern Atlantic resist the cooling caused by the radiative forcing from reduced pCO_2 in the atmosphere. What about carbon? We now know that the model can force lower pCO_2 levels than the observed average glacial values, and that the temperature-pCO_2 correlation breaks in the iron sensitivity experiments. This motivates a closer look into the carbon fluxes between air, sea and land, and what controls their magnitude and direction in the model.

As mentioned in the section *Four feedback pathways*, one of the standing theories about the correlation of pCO_2 and temperature in the paleo-climatological records is that the sea ice and cold conditions lead to uptake of atmospheric CO_2 in the Southern Ocean. The air-sea CO_2 fluxes in the SO, defined as the sum of

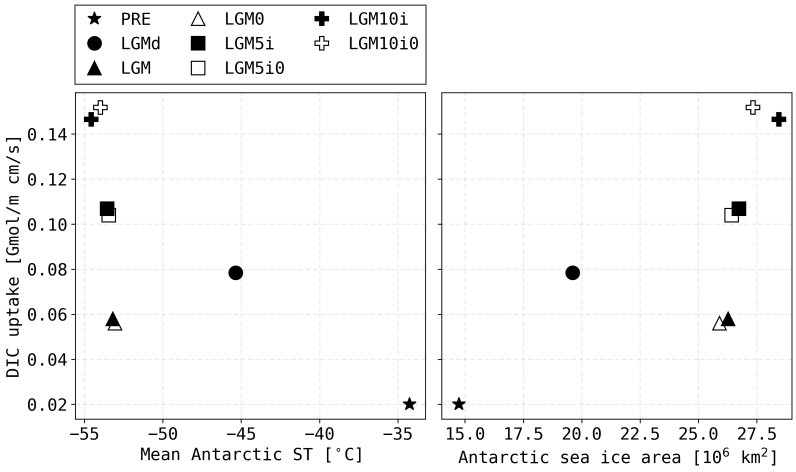

Figure 12: The dissolved inorganic carbon surface gas flux in the SO as a function of mean Antarctic surface temperature (left) and Antarctic sea ice area (right). Uptake is defined as positive.

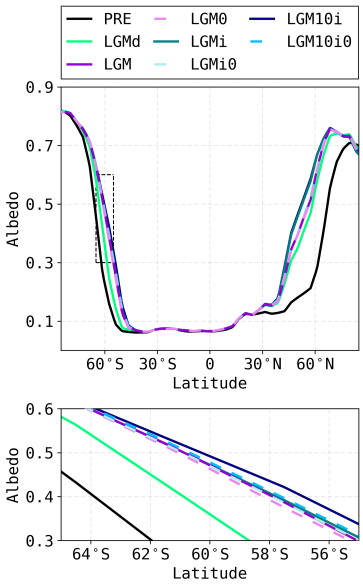

Figure 13: Zonally averaged albedo for all experiments. The black box in the top figure is zoomed in on in the bottom. In the SH, **PRE** and **LGMd** show significant differences in albedo compared to the rest of the experiments, which appear to match exactly. A closer look in the bottom figure reveals that the zero states, **LGM** and **LGM5i** are approximately identical, and **LGM10i** has slightly higher albedo at higher latitudes compared to the other experiments.

all fluxes south of 40°S, plotted against the average Antarctic temperature and the Antarctic sea ice area are given in figure 12. The uptake of DIC in the SO increases with growing sea ice.

LGMd has a relatively high DIC flux rate for its temperature and sea ice extent, as the increased mixing allows for more transfer of carbon between the isopycnal layers. The magnitude of DIC fluxes in the **LGM**, **LGM5i** and **LGM10i** experiments vary significantly despite the low change in the ice extent and temperature, which again results from the experimental design: the phytoplankton activity is enhanced due to iron fertilization.

Zonally averaged albedo gives an indication of how far the ice cover reaches at each experimental steady state (fig. 13). The highest rates of the gas fluxes lay outside of the region covered by 75% or more sea ice, as illustrated in figure 14. In the high concentration sea ice grids, DIC outgassing at low rates dominates. As sea ice becomes more scarce, the flux rates become higher and uptake dominates. The zonally averaged albedo reveals that in the SO, the only stark difference between sea ice extent can be seen between **PRE**, **LGMd** and the rest of the **LGM** experiments. The **LGM**, **LGM5i** and **LGM10i** experiments all exhibit nearly identical albedo zonal average in the Southern Hemisphere (SH). Still, the variation between the DIC flux rates are significantly different. From **LGM0**, to **LGM5i0**, to **LGM10i0**, the regions of uptake in the Indian, Atlantic and Pacific Oceans steadily increase polewards. In **LGM10i0**, the DIC flux is directed into the ocean across nearly the entire region outside of the sea ice range.

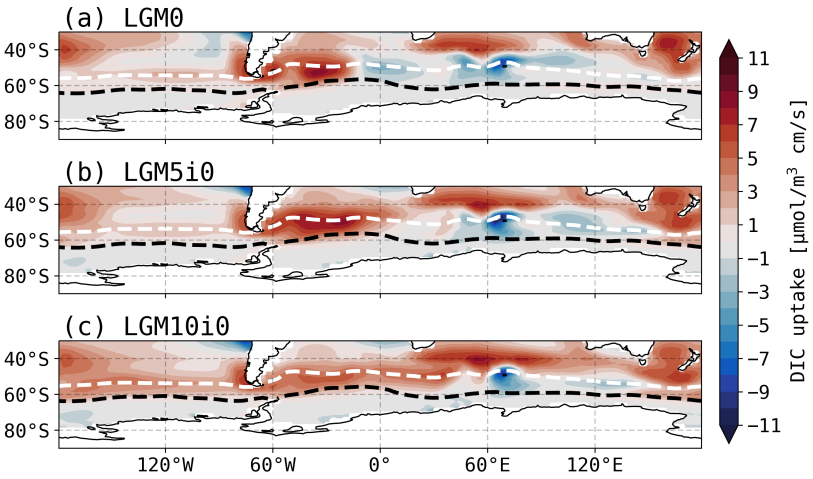

Figure 14: Surface DIC flux in the Southern Ocean in the **LGM0**, **LGM5i0** and **LGM10i0** interstadials. Uptake is defined as positive (red). The white dashed line shows where sea ice covers at least 15% of the grid cells. The black dashed line shows the sea concentration of at least 75%.

The Antarctic sea ice area is plotted as a function of average global temperature in figure 15. There is no break in correlation between temperature and sea ice extent, in other words: no indication that the sea ice growth is too low compared to the magnitude of the drop in temperature.

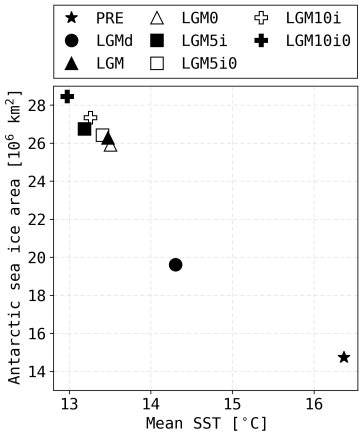

Figure 15: Antarctic sea ice area as a function of the average global temperature.

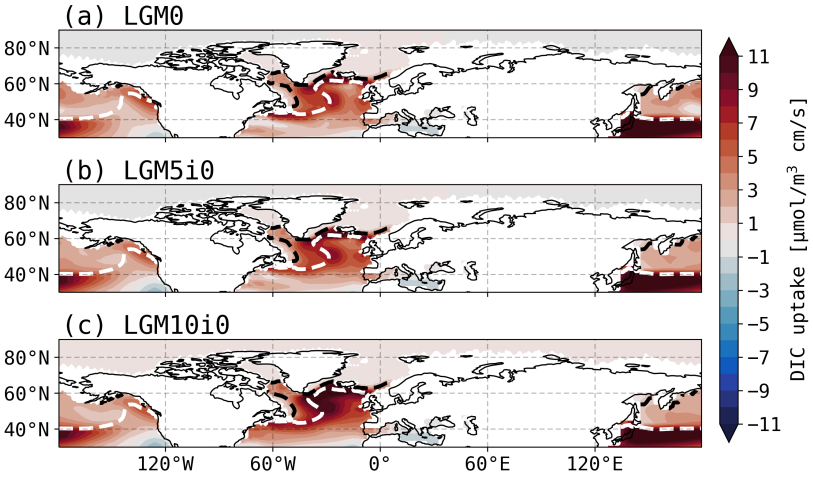

Figure 16: Surface DIC flux in the Northern Hemisphere in the **LGM0**, **LGM5i0** and **LGM10i0** interstadials. Uptake is defined as positive (red). The white dashed line shows where sea ice covers at least 15% of the grid cells. The black dashed line shows the sea concentration of at least 75%.

In the NH (fig. 16), the sea surface region covered by over 75% of ice effectively does not exchange DIC with the atmosphere. In **LGM10i0**, the sea ice retreats due to higher temperatures in the region, which results in higher rates of DIC uptake in the downwelling zone south of Greenland.[21]

It appears that in the SO, the iron fertilization stimulates the soft tissue pump, which results in DIC uptake in the upwelling

[21] The full ice fraction profile in the NH can be viewed in fig. 36 in the Appendix.

Table 3: The magnitude of the effect of the mean temperature on the pCO_2 relative to the **PRE** values: mean ocean temperature of 3.60°C; pCO_2 of 269.2 ppm.

	ΔT [°C]	ΔpCO_2 [ppm]
LGMd	-2.02	-16.2
LGM0	-2.90	-23.2
LGM	-2.97	-23.8
LGM5i0	-2.93	-23.4
LGM5i	-2.79	-22.3
LGM10i0	-2.97	-23.8
LGM10i	-2.98	-23.8

[22] Salinity depends on sea level, constant between the sensitivity experiments

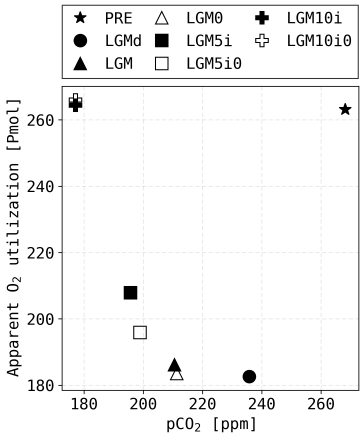

Figure 17: The apparent oxygen utilization global integral in Pmol (peta: 10^{15}) as a function of atmospheric pCO_2.

zone north of the ACC. Sea ice does not seem to reach far enough north to affect the gas exchange in the region. *Eggleston and Galbraith* [2018] use approximations which can estimate the DIC content in the ocean originating from the various pumps outlined in the section *Marine carbon*. In the following analysis, we will look at the relative importance and strength of these pumps to confirm that the air-sea carbon fluxes are fully understood.

Solubility: DIC_{sat}

Colder sea water can hold more DIC, and therefore a fraction of the pCO_2 gone from the atmosphere is due to this effect. *Jochum et al.* [submitted] have estimated that a 2.5°C drop in mean ocean temperature corresponds to about 20ppm drop in the atmospheric CO_2. In all of the experiments, the salinity is 1 psu higher, which is counted into the calculation[22]. Table 3 lists the decrease in average ocean temperature (ΔT) for all of the experiment with respect to **PRE**, and the corresponding uptake of the atmospheric CO_2 (ΔpCO_2) due to solubility. In all of the steady state averages except for **LGMd**, ΔT ranges between -2.79 and -2.98°C, which results in a nearly identical DIC_{sat} content.

Apparent O_2 utilization: DIC_{soft}

In the process of organic material dissolution in the water column to produce DIC_{soft}, oxygen is consumed. *Eggleston and Galbraith* [2018] approximate DIC_{soft} with:

$$DIC_{soft} = r_{C:O_2} \cdot (O_{2_{pre}} - O_2),$$

where $r_{C:O_2}$ is 117/138, and $O_{2_{pre}} - O_2$ is the difference between preformed oxygen and the oxygen saturation of the water parcel at the time of subduction. Figure 17 displays the global integral of this difference termed apparent oxygen utilization (AOU) as a function of atmospheric pCO_2. The model output indicates that the **PRE** ocean is filled with more DIC_{soft} than the **LGM** and the **LGM5i** ocean. The soft-tissue pump only becomes slightly stronger than in the pre-industrial setup when the aeolian dust fluxes are increased tenfold.

The mean depth and mean zonal AOU for **PRE**, **LGM0** and **LGM10i0** can be found in the Appendix in figures 39 and 40, re-

spectively. Generally, there is least DIC_{soft} in the Atlantic and its concentration steadily increases towards the SO, with maximum values in the equatorial and northern Pacific. This distribution is a reflection of the patterns of biological activity in the ocean, as well as of its overturning currents: the DIC_{soft} from all ocean basins ends up mixed in the ACC, but the portion which feeds into the Atlantic ends up getting utilized at the surface. Generally, the **LGM10i** experiment stabilizes at the highest DIC_{soft} content globally, followed by **PRE** and **LGM5i**. The only region where the DIC_{soft} content exceeds **LGM10i0** in **LGM0** is around the North Pole, where NADW is formed.

In figure 18, the integral of the SO DIC uptake is plotted against the AOU. The DIC_{soft} marine content is correlated with the sea-air flux rate of DIC, except **PRE**, which has the highest relative DIC_{soft} content and the lowest rate of DIC uptake. The **LGM** setup has a considerably lower carbon inventory in the system. However, still it is generally agreed that the soft-tissue pump was stronger during the glacials. The low content of DIC_{soft} in the ocean is affected by deep water formation rates, as discussed in the following section about DIC_{dis}.

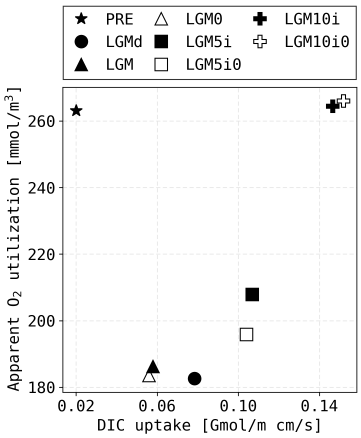

Figure 18: The AOU global integral as a function of the Southern Ocean integral of DIC flux rate in Gmol/m cm/s (giga: 10^9).

NADW and AABW strenght: DIC_{dis}

Eggleston and Galbraith [2018] estimate the DIC_{dis} content using:

$$DIC_{dis} \approx f_{AABW} \cdot DIC_{dis}^{AABW} + (1 - f_{AABW}) \cdot DIC_{dis}^{NADW},$$

where f_{AABW} is the fraction of water mass below 1000 m which constitutes of AABW, and $1 - f_{AABW} \approx f_{NADW}$.

Although calculating the DIC_{sat} in the ocean waters is outside the scope of this project, *Jochum et al.* [submitted] find that the relative strength of the NADW and AABW cells is indicative of the DIC_{dis} content in the ocean, and can also aid to explain the DIC_{soft} distribution. Figure 19 shows the residual meridional overturning circulation in the Atlantic and Southern Oceans. The maximum of volume transport in the AMOC cell indicates the NADW formation strength, while the minimum in the bottom SOMOC cell indicates the AABW formation strength. Compared to **PRE**, in **LGM0**, **LGM5i0** and **LGM10i0**, both the AABW and

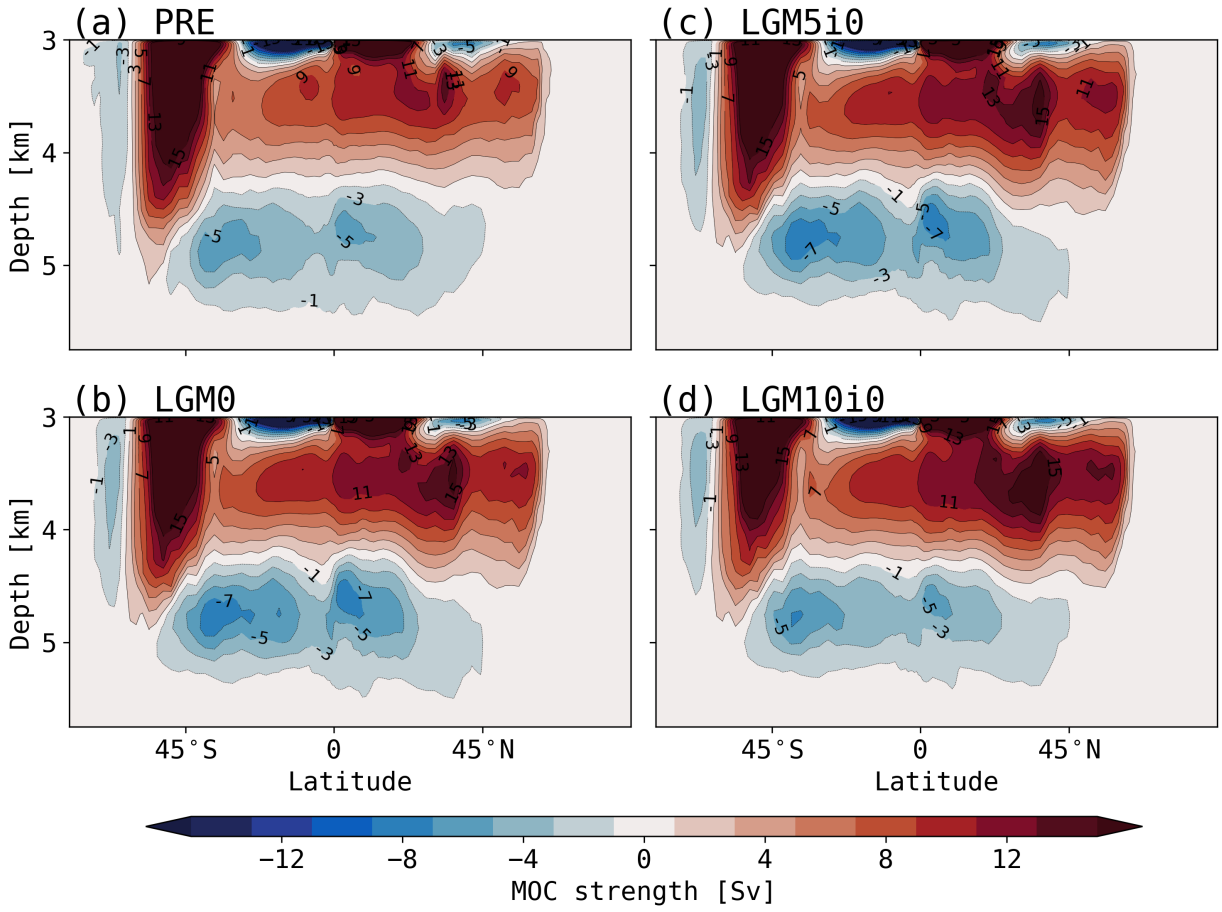

Figure 19: MOC residual in the Atlantic and Southern Oceans for (a) **PRE**, (b) **LGM0**, (c) **LGM5i0** and (d) **LGM10i0**. Blue indicates anit-clockwise circulation, while red: clockwise.

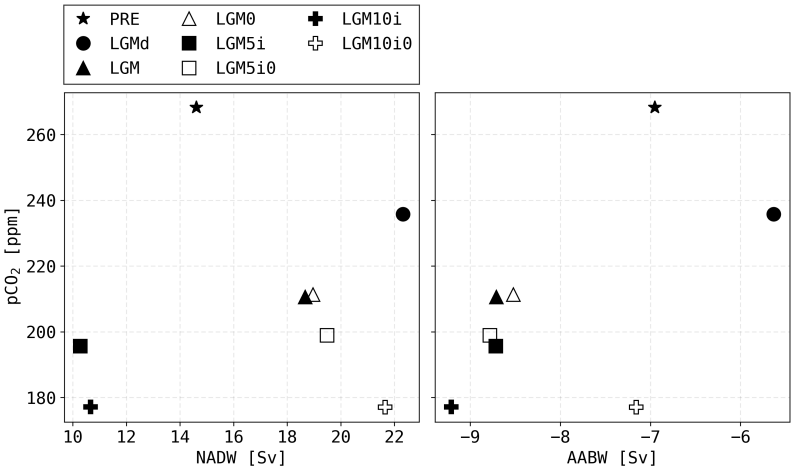

Figure 20: NADW and AABW formation strength as functions of pCO_2.

NADW formation is increased. Figure 20 reveals that between the steady states in the iron fertilization experiments, the NADW formation is strongest in **LGM10i0** and weakest in **LGM0**. In the case of the AABW formation, the bottom cell is the strongest in **LGM5i0** and the weakest in **LGM10i0**.

The AABW formation weakens significantly in the **LGM10i** interstadial. The plot also illustrates the challenge in dealing with the D-O events. One of the signature properties of stadials is the AMOC shut down, which is seen clearly in the NADW formation strength plot. This makes it difficult to make any conclusions about the impact of the MOC cell strengths on the DIC_{sat} content in the ocean.

DIC: summary

Figure 21 shows the total marine DIC content for all experiments. In the LGM sensitivity experiments, 1480 PgC is locked in the inert pools [*Jochum et al.*, submitted], which results in 780 PgC drop in marine DIC content between **LGM** and **PRE**.

Solubility does not contribute to the variability in the marine carbon content between the **LGM** and iron sensitivity experiments, as the ocean temperature does not vary significantly between them. DIC_{sat} only shows significant change between **LGMd** and **LGM**.

The marine dissolved inorganic carbon content is lowest in **LGMd**, as the doubled isopycnal diffusivity allows for higher rates of CO_2 exchange with the atmosphere. It is also the exper-

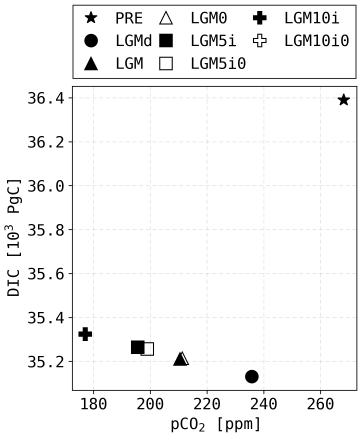

Figure 21: Global integral of total marine DIC content as a function of pCO_2.

iment with strongest NADW formation and weakest AABW formation. This is, too, due to the increased diffusivity: the NADW cell becomes deeper as more cold, heavy water from the AABW cell in the Northern Atlantic is allowed to mix with the cell above. Simultaneously, AABW loses volume in the NH and becomes weaker.

The strengthening of the cells makes it more difficult for the DIC_{soft} to sink into the water column, and instead it is re-cycled in the surface ocean. Therefore, while we get more phytoplankton activity in the SO due to iron fertilization, the soft tissue pump is still weaker in **LGM5i0** than in **PRE**. The highest content of DIC is present in **LGM10i0**. The tenfold increase in iron dust stimulates the phytoplankton, but the DIC_{soft} is also allowed to sink due to the low strength of AABW in this experiment's interstadial. Although it appears that increasing DIC_{dis} content could potentially be correlated with decreasing pCO_2 levels, the results are inconclusive due to the additional processes which appear with D-O oscillations.

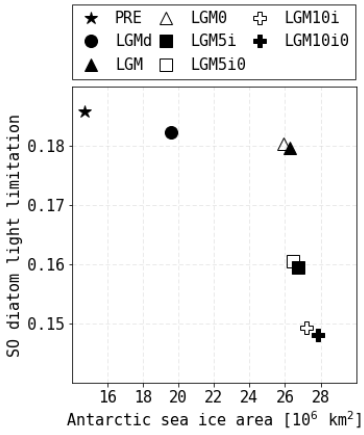

Figure 22: The light limitation of diatoms in the Southern Ocean as a function of Antarctic sea ice area.

Marine biogeochemistry

There are three functional phytoplankton groups in the BGC component of CESM, and two of them are light limited in the Southern Ocean: small phytoplankton (sp) and diatoms. Figure 22 shows the mean light limitation for diatoms in the SO, where 0 corresponds to maximum limitation of growth, and 1 to no limitation resulting from access to light. The SO limitation is calculated by finding the weighted mean value across all longitudes and latitudes South of 40°S, and across the 150m depth of the surface water.

Regardless of a large difference in sea ice extent, diatoms experience nearly the same light limitation in the **PRE**, **LGMd** and **LGM** experiments. The phytoplankton is more limited by light in the **LGM5i** experiment, and most light limited in the **LGM10i** SO, which corresponds to the highest sea ice concentration. The correlation between the light limitation and sea ice area breaks with the **LGM** experiment. The phytoplankton is highly sensitive to small changes in the ice fraction, as illustrated by figure 23. The ice expansion of the LGM conditions and the polar night

already make this a challenging environment for phytoplankton growth, which is evident from the average light limitation value of 0.18. The expanding ice in **LGM5i0** and **LGM10i0** does not have a significant signature in the zonal albedo comparison (fig. 13). Nevertheless, the ice fraction does change: in **LGM5i0** by maximum of 0.06, and in **LGM10i0** by 0.1 or less (the full comparison of ice fraction values in the SO between these interstadial averages can be found in figure 37 in the Appendix). This change is enough to decrease the average light limitation down to 0.15 in **LGM10i0**, as the regions of increased ice fraction highly correlate with the patches in the SO where the growth of diatoms becomes more light limited.

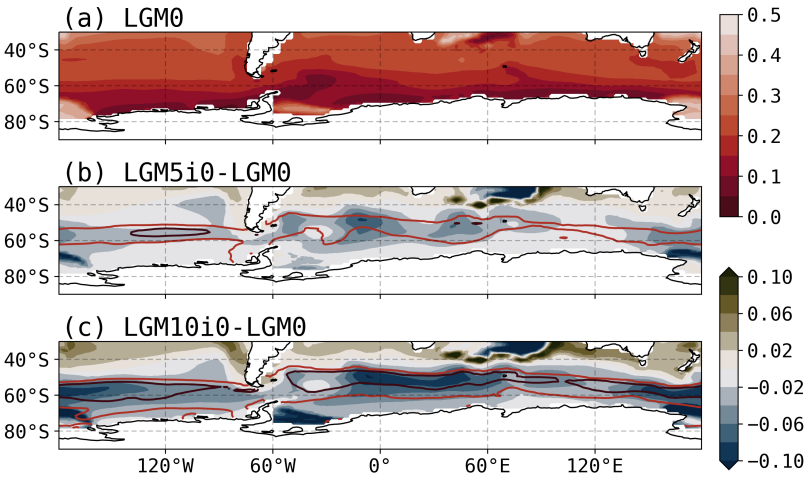

Figure 23: Light limitation for diatoms in the southern ocean in (a) **LGM0**, and the difference in light limitation (b) **LGM5i0-LGM0** and (c) **LGM10i0-LGM0**. The contours in (b) and (c) show the difference between the ice fraction in **LGM5i0-LGM0** and **LGM10i0-LGM0**, respectively. The light red contour corresponds to 0.01 increase, and the dark red contour to 0.04 increase in ice fraction.

Fertilized diazotrophs

Diazotrophs are at the heart of the **(CC^{b})** hypothesis, as the species *Trichodesmium* dies out when background pCO_2 levels reach below 180 ppm [*Hutchins et al.*, 2013].

The model diazotrophs are not pCO_2 limited, but temperature limited [*Moore et al.*, 2004], as the only phytoplankton group with such limitation. This is done to reflect the observed distribution of *Trichodesmium*, which is only found in waters of temperature above 20°C. In figure 26, the diazotroph chlorophyll distribution is presented, where the cultures live exclusively at low latitudes. Knowing this, we cannot be fooled by figure 24, which shows the global diazotroph concentration integral as a function of pCO_2. The chlorophyll peaks at **LGM5i0**, and then drops drastically as

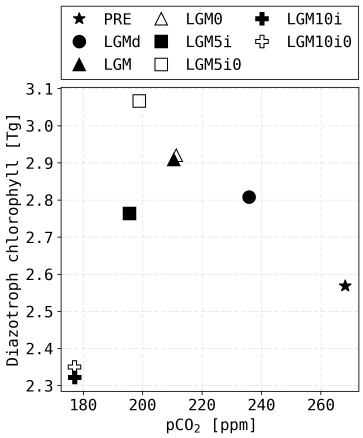

Figure 24: The concentration of diazotroph chlorophyll in the ocean in Tg (tera = 10^{12}) as a function of atmospheric pCO_2.

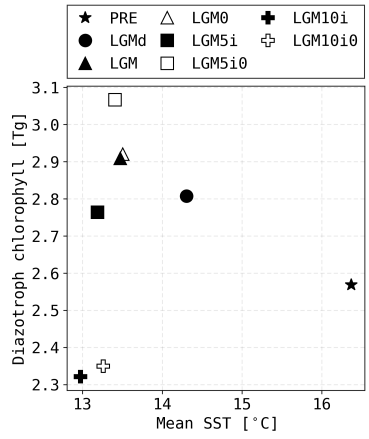

Figure 25: The concentration of diazotroph chlorophyll as a function of sea surface temperature.

the limit of 180 ppm is crossed in **LGM10i**. However, as we know, the limit is not implemented in the model. What else could cause this decrease?

In figure 25, the diazotroph chlorophyll concentration is plotted against the sea surface temperature instead. Temperature could be a safe bet, since the model diazotrophs are limited by it. However, the **LGM**, **LGM5i** and **LGM10i** experiments have a similar SST compared to the vastly different diazotroph concentrations. A closer look at diazotroph distribution in the ocean in figure 26 shows another possible explanation, which ties in with the surface nutrient transport in the Atlantic.

Figure 44 in the Appendix shows the effect of increased aeolian dust transports on iron limitation for diazotrophs. This phytoplankton group is heavily iron limited, and the iron fertilization causes a significant increase in its chlorophyll between **PRE** and **LGM10i** in the Pacific. Interestingly, the diazotroph chlorophyll drops in the Atlantic and Indian Oceans in **LGM10i** compared to **PRE**. In fact, the most diazotroph abundance in these regions can be seen in **LGM0**, which is somewhat contrary to expectation, as the diazotrophs' growth is as limited by iron as in **PRE**. Additionally, figures 24 and 25 show that although the ocean is fertilized with iron tenfold in **LGM10i** compared to **PRE**, the total diazotroph concentration drops below that of **PRE**.

As outlined in the section *World's Ocean*, the AABW is typically oversaturated with DIC, while NADW is undersaturated. Due to the HNLC nature of the Southern Ocean region, before the surface waters flow out of the ACC, the nutrients from the abyss are utilized by the phytoplankton residing there. The remaining nutrients travel with the flow in the surface waters of the Atlantic and get utilized by phytoplankton living at low latitudes. This balance indicates that there could exist a state in which all the nutrients get utilized before they even reach the Atlantic surface waters. This state was previously observed in model studies, including in the output analyzed in this project [*Möllney*, 2020; *Moore et al.*, 2018] and is termed *nutrient trapping*. Möllney finds that the iron fertilization in **LGM5i** leads to higher nutrient consumption in the Southern Ocean, which in turn has significant implications for export production north of 30°S. Figure 43 in the Appendix aligns with the expectations for

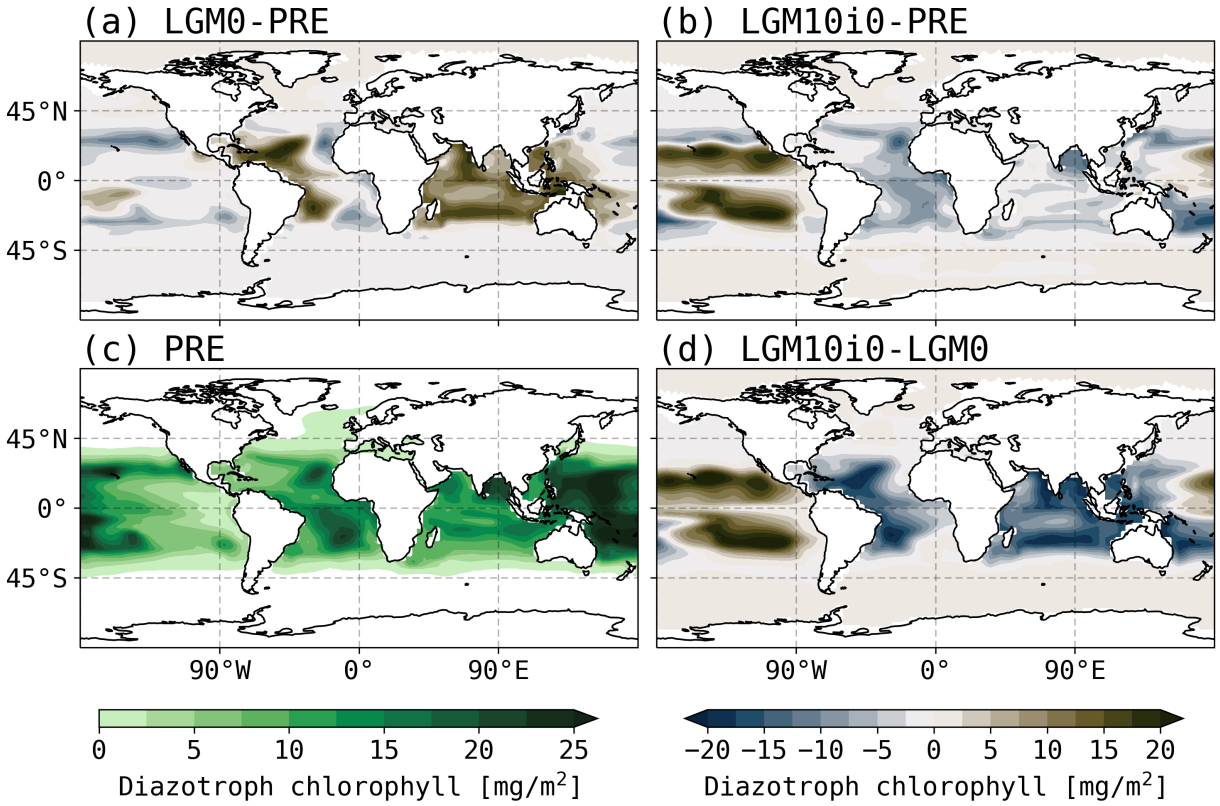

Figure 26: The depth integral of diazotroph chlorophyll concentration for all grid points in (a) the difference **LGM0-PRE**; (b) **LGM10i0-PRE**; (c) **PRE** and (d) **LGM10i0-LGM0**.

the nutrient trapping: the phosphate limitation for diazotrophs is low in the Atlantic and Indian Oceans, reaching a minimum of 0.5. In **LGM10i0**, the diazotrophs experience 10 to 30% higher limitation due to phosphate availability compared to **PRE**.

In order to take a closer look at this potential negative feedback, we need to analyze the patterns of particulate organic carbon in the ocean.

Nutrient trapping

In **LGM0**, more POC rains down in the equatorial Pacific, the entire Atlantic and Indian Oceans, but there is generally less POC rain in the Southern Ocean compared to **PRE** (fig. 27). The **LGM10i0** map illustrates the effect of iron fertilization in the Southern Ocean, as we see significantly intensified POC rain in this region. The equatorial Pacific also sees more particulate inorganic carbon compared to both **LGM0** and **PRE**, however the **LGM10i0** experiment shows a stark decrease in POC rain in the Atlantic and Indian basins compared to **LGM0**.

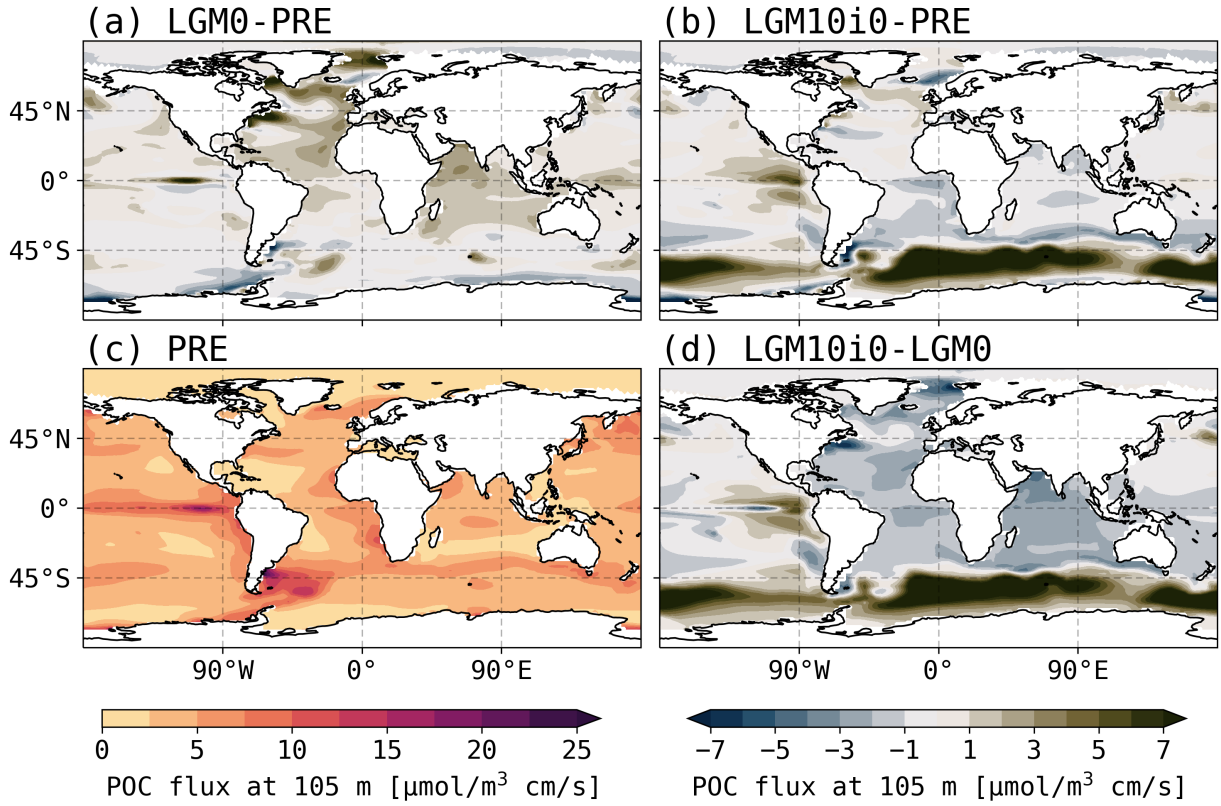

Figure 27: The particulate organic carbon flux at 105 meters for the entire ocean: (a) **LGM0-PRE**; (b) **LGM10i0-PRE**; (c) **PRE** and (d) **LGM10i0-LGM0**.

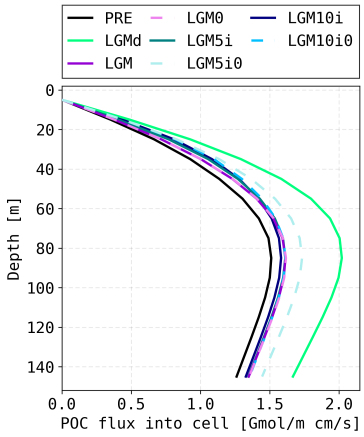

Figure 28: Particulate organic carbon flux global integrals as functions of the depth of the surface ocean.

Figure 28 shows the POC flux global integrals varying with depth. The flux increases down the water column until 80m, where the phytoplankton concentration reaches its maximum. Below that, the flux is gradually decreasing, due to recycling of the material inside the euphotic zone, scavenging and dissolution. The POC variable in the model is only calculated down to 150 meters, however theoretically, we'd see POC decreasing over the entire water column, gradually nearing to zero again.

It is immediately apparent that **PRE** and **LGMd** are the two most standing-out experiments again in terms of the export production. We see the least of the POC rain in **PRE** at all depths, and the most of it in **LGMd**: the doubled diffusion coefficient, mimicking increased tidal mixing, allows more matter to transfer between the isopycnals. Apart from these two experiments, we also have **LGM**, and **LGM5i** and **LGM10i** stadials, which follow nearly identical pattern across all depths, similar to **LGM0** and **LGM10i0**. The two iron fertilization experiment interstadials show an interesting feature which further points towards the pos-

sible nutrient trapping effect: the export production in **LGM5i0** is higher than in **LGM10i0**.

This is striking, as we've seen before that **LGM10i0** ocean contains more DIC_{soft} and the atmospheric pCO_2 is lower compared to **LGM5i0**. We also get higher DIC uptake in the Southern Ocean in the **LGM10i0** experiment, despite phytoplankton being more light limited compared to **LGM5i0**. Figure 29 shows that the export production peaks at **LGM5i0**, and then decreases again, even as more carbon is utilized by the phytoplankton in the Southern Ocean. Combined with 27, it appears that the loss of phytoplankton in the Atlantic Ocean can potentially outweigh the effect of iron fertilization in the SO. It is not drastic enough to decrease the marine DIC_{soft} content, but perhaps an even higher dust flux could achieve this.

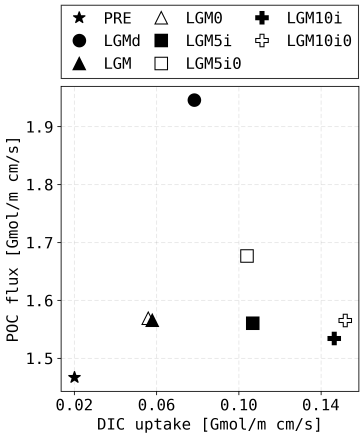

Figure 29: The global integral of POC flux at 105 meters as a function of the total uptake of DIC in the Southern Ocean.

Land carbon

The **(CC^a)** hypothesis postulated by G&E suggests that a negative feedback involving the land carbon reservoir is responsible for maintaining the pCO_2 levels above the 190 ppm threshold. The average Antarctic temperature and average global temperature as functions of total terrestrial carbon are showed in figure 30. Due to the removal of carbon from the Earth system into the inert pools, the total column C drastically decreases between **PRE** and the LGM experiments.

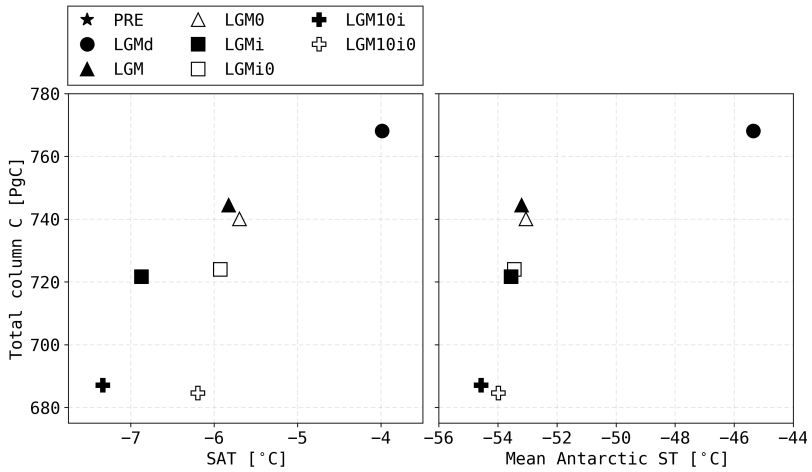

Figure 30: Mean surface temperature (left) and the average Antarctic temperature (right) as functions of total terrestrial carbon. The **PRE** experiment output values for these variables are significantly higher than the rest of the experiments, hence they are not included in the figure. The **PRE** values are: 1324 PgC of the total global land carbon content, mean SAT of 1.1°C and mean Antarctic SAT of -34.2°C.

The land carbon reservoir decreases with dropping temperatures, as expected. The land system loses vegetation at higher

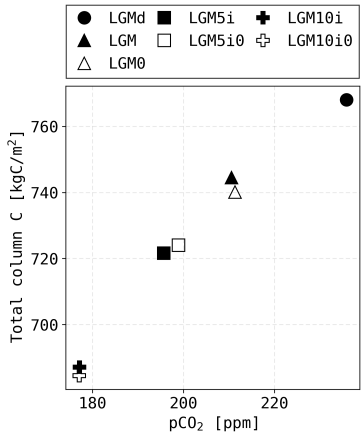

Figure 31: Total column carbon global integral as a function of pCO_2 for all experiments except for **PRE**.

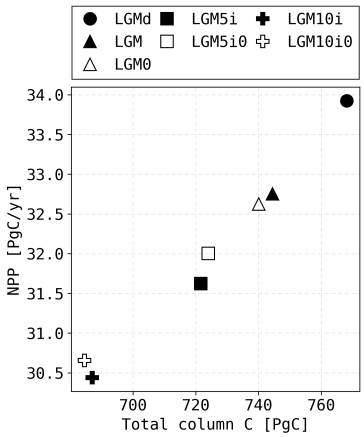

Figure 32: Global NPP rate as a function of pCO_2 for all experiments except for **PRE** (**PRE** NPP = 48.5 PgC/yr).

rates under decreasing global temperatures: from **LGMd** to **LGM0**, there is almost a 2°C drop in globally averaged SAT, which results in about 30 PgC drop in land carbon content. In contrast, about 40 PgC is removed from land in **LGM10i0** compared to **LGM5i0**, while the SAT only drops by 0.3°C. This suggests that an additional physical property, aside from temperature, is causing vegetation to die out in the iron sensitivty experiments.

Figure 31 shows the correlation between the atmospheric CO_2 and the total global land carbon reservoir. Similarly to the case with diazotrophs, we could easily be fooled by this plot have we not known that there is no background limitation of photosynthesis in the CESM1 land component. Instead, figure 33 illustrates the strong correlation between the precipitation and the land carbon content in the model. The changes in these variables are of much lower magnitude between **LGM10i0** and **LGM0**, compared to **PRE** vs. **LGM0** (fig. 34). Precipitation rates can explain some, but not all carbon storage loss in **LGM10i0**. A most prominent example of this can be seen over Europe and Western Asia, as well as patches of South and North Americas.

Figure 38 in the Appendix completes the picture, as the aforementioned patches lay in regions of significant SAT decreases. It is clear that, as per model design, soil moisture and temperature control the land carbon concentration, and background pCO_2 levels have no influence on photosynthesis. Interestingly, figure 32 reveals that the lowest global NPP rates in the model output fall right above the confidence bracket of glacial NPP values estimated from observations, cited by *Ciais et al.* [2012] as (20±10) PgC/yr.

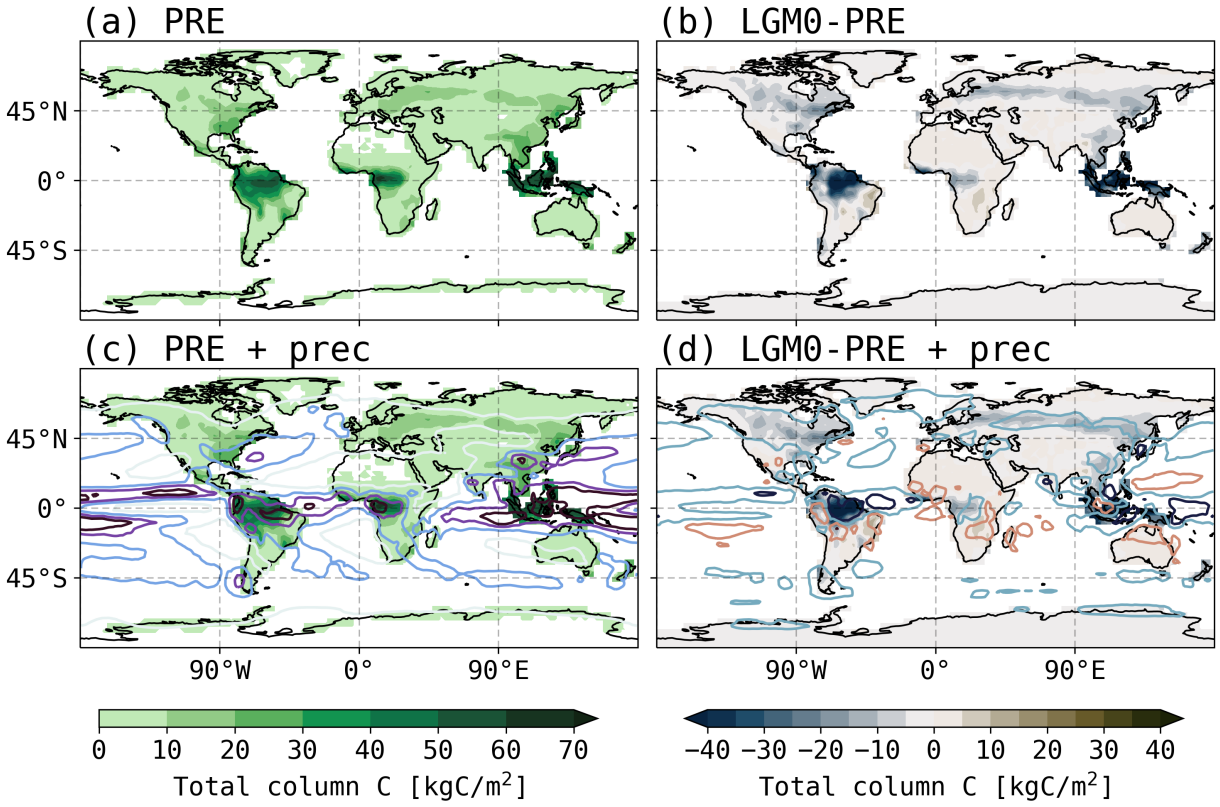

Figure 33: The distribution of column carbon concentration in (a) **PRE** and (b) **LGM0-PRE**. The C maps are overlaid with the contours of precipitation patterns. In (c), the precipitation rate of **PRE** is pictured, where the contours correspond to 1 mm/day (white), 3 mm/day (blue), 5 mm/day (light purple) and 7 mm/day (dark purple). In (d), the contours show the preciptiation rate of **LGM0-PRE**, where the light blue contour corresponds to 1.5 mm/day decrease in precipitation, dark blue shows 5 mm/day decrease, and light red shows 1.5 mm/day increase.

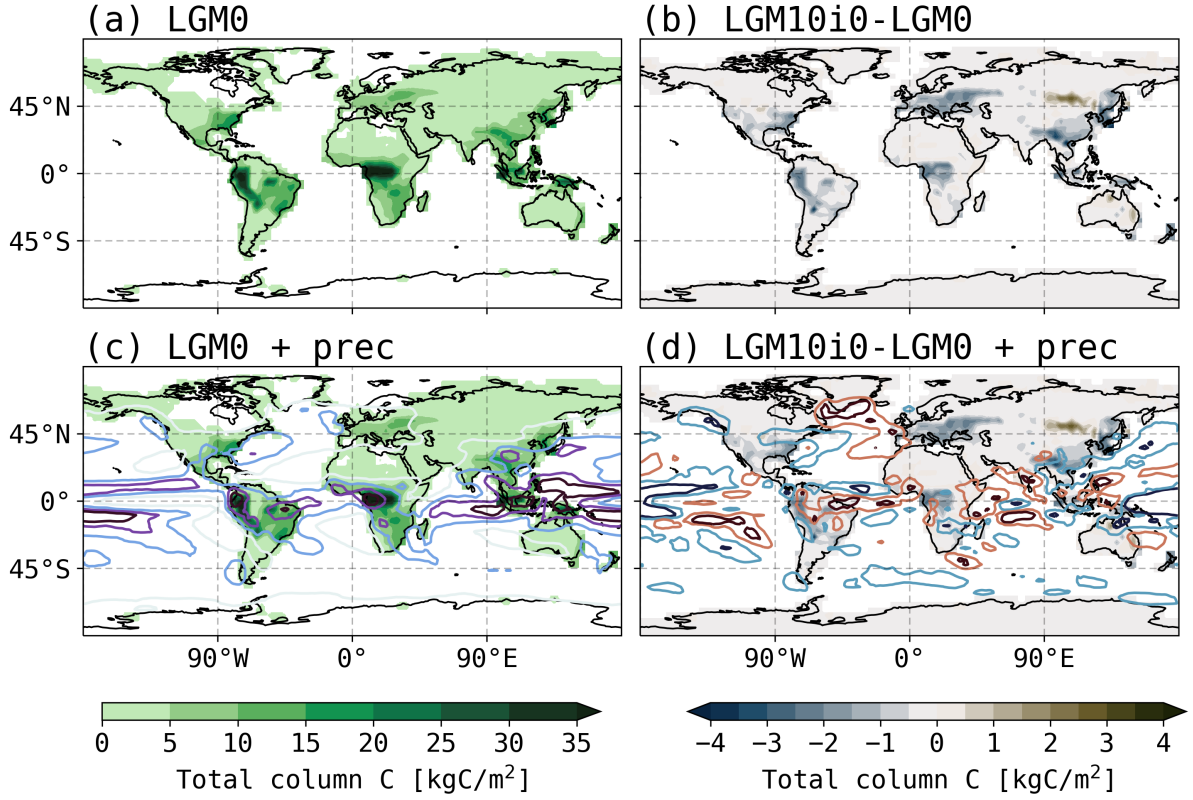

Figure 34: The distribution of column carbon concentration in (a) **LGM0** and (b) **LGM10i0-LGM0**. The C maps are overlaid with the contours of precipitation patterns. In (c), the precipitation rate of **LGM0** is pictured, where the contours correspond to 1 mm/day (white), 3 mm/day (blue), 5 mm/day (light purple) and 7 mm/day (dark purple). In (d), the contours show the preciptiation rate of **LGM10i0-LGM0**, where the light blue contour corresponds to 0.08 mm/day decrease in precipitation, dark blue shows 0.2 mm/day decrease, light red shows 0.08 mm/day increase and dark red: 0.2 mm/day increase in precipitation rates.

Summary

The atmospheric CO_2 concentration is correlated with temperature (fig. 9), however this correlation breaks with the iron fertilization experiments. Increasing the aeolian dust transport fivefold leads to about 12 ppm decrease in pCO_2, and increasing it tenfold leads to 34 ppm decrease. Despite this drop in radiative forcing from CO_2, the mean ocean temperatures remain effectively unchanged. Figure 12 demonstrates that the uptake of DIC generally increases as temperatures fall and the Antarctic ice grows. Global patterns of DIC flux are showed in the Appendix in figure 46, and they reveal that carbon uptake from the atmosphere is increased mainly at the poles and in the equatorial Pacific. Figures 14 and 16 afford a closer look into the polar regions, which are interesting for each their own reason: in the Northern Hemisphere, a hot pocket (fig. 11) causes ice in the Northern Atlantic to melt, which allows more carbon exchange with the atmosphere; in the Southern Ocean, iron fertilization stimulates the soft-tissue pump and transforms the outgassing-dominated DIC upwelling zone into an uptake region.

The breakdown of the DIC components illustrates that the deep water formation strengths are key in the changed uptake patterns (figs. 19 and 20). In the Northern Hemisphere, the vigorous AMOC is likely the reason for the heat transport into the Northern Atlantic. In the Southern Hemisphere, the SOMOC in **LGM10i0** is significantly weaker than in **LGM5i0** and **LGM0**, which allows for more DIC_{soft} to accumulate in the abyss. All of the iron sensitivity experiment stadials, together with **LGM0**, see more vigorous deep water formation cells compared to **PRE**, resulting in lower ideal age values[23] (figs. 41 and 42 in the Appendix). The NADW and AABW formation strengths have conflicting influence on the marine DIC content: on one hand, higher rates of deep water formation increase the marine DIC_{dis} content; on the other, faster circulation prevents DIC_{soft} from sinking into the abyss. This could potentially explain why **LGM10i0** has a higher DIC_{soft} content than **LGM5i0**, despite lower export production (fig. 28).

Regions with high ice fraction (>75%) in the NH suppress the sea DIC exchange with the atmosphere completely (fig. 16). In

[23] Ideal age (IAGE) is a value defined as the time from the point at which a water parcel was last in contact with the atmosphere.

the SH, the highest concentrated sea ice covers the downwelling zone of the SO, the region where we see weak DIC uptake in **PRE** (fig. 4 in the Appendix). The capping effect supresses this exchange and contributes to pCO_2 outgassing. The light attenuation effect in the region of upwelling north of the ACC would decrease the phytoplankton activity without the iron fertilization, as the autotrophs become more light limited with extending sea ice (fig. 22).

The marine biogeochemistry patterns reveal that nutrient trapping occurs: the nutrients get utilized in the Southern Ocean as the iron limitation is lifted, and the depleted surface waters flow into the Atlantic and Indian basins, causing a reduction in phytoplankton growth. This results in reduced export production in **LGM10i0** compared to **LGM5i0**, despite higher aeolian dust fluxes, which in turn causes a dramatic drop in diazotroph chlorophyll in **LGM10i0** (fig. 25). On land, there appears to be a carbon feedback (fig. 31), however the pCO_2 photosynthesis limit does not exist in the model. The analysis reveals that it is the precipitation and temperature patterns which reduce total land carbon between **LGMd**, **LGM0**, **LGM5i0** and **LGM10i0** (fig. 34 and fig. 38 in the Appendix).

Connecting the dots

After two journeys through time and space on Earth, one in the real world and another in the model realm, your head is probably filled to the brim with ideas. It's time to reflect on what we have learned, and assess how useful this new knowledge is in the bigger picture. In this second to last chapter, I will compare the model output to existing observations, review the four feedback pathways and their signal in the model, outline the challenges of testing said pathways in CESM1 and propose how the work on understanding the carbon cycle could be continued in the future. Buckle up! We're almost there.

Model verification

A multitude of biases exist in CESM1, which is to be expected in a simulation of such complexity. Nevertheless, it is able to capture key components of the climate system, both in the present and under the LGM conditions.

The estimate of the pre-industrial pCO_2 level is usually cited as 280 ppm, while the LGM values lay around 190-200 ppm [e.g. *Neftel et al.*, 1982; *Peacock et al.*, 2006]. The model value in **PRE** for mean pCO_2 is below the pre-industrial estimate of 269.1 ppm, while in **LGM0** we get a higher value of 211.7 ppm. The **LGM5i** comes closest to the LGM pCO_2 level estimate, with mean values of 196.0 ppm during the stadial and 199.2 ppm in the interstadial. The drop in the mean ocean temperature between **LGM** and **PRE** is of 2.97°C, remarkably close to the estimate of (2.57 ± 0.24)°C by *Bereiter et al.* [2018] based on ice core reconstructions. The SAT decrease between the two experiments amounts to 6.95°C, about 2°C higher than the upper bracket of the reconstructed value of (4.0 ± 0.8)°C [*Annan and Hargreaves*,

2013].

The modeled LGM does not agree with a number of past reconstructions of deep water flow. One of the least disputable observations about the glacial overturning circulation is the shallower AMOC cell [e.g. *Lynch-Stieglitz et al.*, 2007], which is not reproduced in the model (fig. 19, section *Temperature and carbon*). Fortunately[24], this appears to be the only property of the glacial overturning circulation that experts in the field agree on. *Du et al.* [2020] outline some of the highly debated points on the topic: the mixing proportions of water parcels sourced in the North versus the South in the deep Northern Atlantic; the AMOC strength during the deglacial stadials; the magnitude and direction of AMOC and SOMOC responses to glacial conditions; and potential changes in the Pacific circulation. The overturning circulation is thought to have weakened due to changes in the Southern Westerlies [*Toggweiler et al.*, 2006]. From their own proxy results, *Du et al.* [2020] find that during the glacial, both AMOC and SOMOC strengths were reduced compared to the present, resulting in longer ideal age values for abyssal waters. In contrast, *Lynch-Stieglitz et al.* [2007] find that the overturning strength was approximately the same as today. In this study, IAGE in **LGM0** and **LGM10i0** is lower than in **PRE** (figs. 42 and 41 in the Appendix), and the overturning cells strengthen compared to **PRE**, except **LGM10i0**, where the AABW formation is nearly identical in strength to the pre-industrial setup (figs. 19 and 20 in section *Temperature and carbon*).

Galbraith and Skinner [2020] outline the difficulties of considering properties of biogeochemical cycles in the glacial Earth. There are no direct ways of reconstructing the DIC content in the past climates. The inventory of nitrogen, which is one of the two major limiting nutrients in marine ecosystems next to iron, is also difficult to asses. There are multiple processes which offset the inventory in opposite directions[25]. The soft-tissue pump in the LGM has been generally considered to have been stronger, but with a caveat that the processes involved are still poorly understood [*Hain et al.*, 2014]. In their LGM simulations, *Galbraith and Skinner* [2020] find a decreased export flux despite iron fertilization, similarly to the difference between **LGM5i0** and **LGM10i0** in this study. Aside from the disagreement with the

[24] (For the modellers.)

[25] An example of this is the problem with diazotrophs and background pCO_2 levels: the cultures are highly phosphate limited; this limitation is lifted during the LGM, but low pCO_2 levels limit their growth again. The magnitude of each of these effects is uncertain.

soft-tissue pump strength, there exists a well-known issue with the CESM1 BGC component: overestimated oxygen minimum zones and a negative SO ventilation bias [*Lindsay et al.*, 2014]. Our problem with oxygen does not end there. AOU is commonly used to estimate the DIC_{soft} content in the deep ocean. The assumption is that the atmospheric and sea surface O_2 is in equilibrium, which turns out to be poor in the regions of deep water formation [*Ito et al.*, 2004; *Bernardello et al.*, 2014]. *Khatiwala et al.* [2019] quantify the resulting error on the true respired oxygen in the ocean, estimating that the disequilibrium oxygen might result in as much as 50% of respiration overestimation when using the AOU approximation. This results in a large underestimation in the DIC_{soft} content. Ergo, the model limitations and the AOU approximation compound, and as a result our modeled DIC_{soft} is likely significantly underestimated.

Möllney [2020] conducts an excellent discussionn on the effects of iron fertilization in the **LGM5i** experiment and compares them to the existing reconstructions. Figure 35 shows the summary of this discussion and illustrates her conclusions: the model generally agrees with the observations in the Southern and the Indian Oceans, but shows a positive bias in export production in the Pacific and a negative bias in the Atlantic. Moreover, **LGM5i** exhibits an improvement in matching the observations in the upwelling zone of the Southern Ocean.

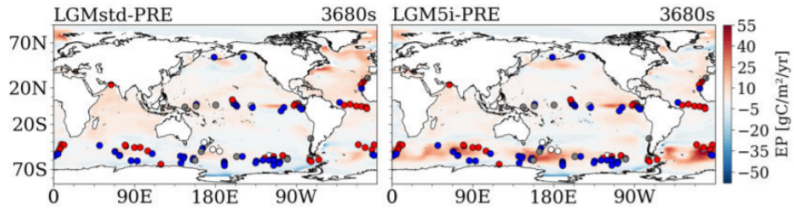

Figure 35: The comparison of the proxy record for C export (marked in red, blue, white and gray dots) to the model output. Left shows the map for export production in the experiment **LGM-PRE** and right: **LGM5i-PRE** in a 10 model year average of 3680s. The reconstructions compare the export production in LGM to early Holocene, where red signifies higher, blue lower export production, white signifies no change and gray is ambiguous. Figure source: *Möllney* [2020].

The global dust flux estimates in the LGM stretch over a wide range. *Jickells et al.* [2005] review multitude of studies on iron fertilization and report that aeolian dust fluxes are estimated to have been 2 to 20 times higher during the last glacial. *Lambert et al.* [2015] break down the estimates into locations and note that globally, the dust fluxes are generally thought to have been 3 to 4 times higher, however only 2 to 3 times higher in the Pacific and up to 30 times higher in the polar regions. In the **LGM5i** and

LGM10i experiments, the dust fluxes are increased uniformly everywhere. This could be why *Möllney* [2020] finds a better agreement in sediment core reconstructions in the SO, but a positive bias in export production in the Pacific.

The modern estimates of the terrestrial NPP range from 48.0 PgC/yr to 69.0 PgC/yr [*Gough*, 2011][26], hence it appears that the **PRE** value for pre-industrial NPP of 48.5 PgC/yr is sensible. The NPP in **LGM** is 32.8 PgC/yr, impressively close to the estimates from observations of (20±10) PgC/yr, considering that the model does not include a number of features seen in the terrestrial biosphere: there is no dependence of photosynthesis, nor of stomatal conductance on background pCO_2 levels; the C/N ratios are fixed, meaning that plants cannot adapt to low nutrient supply. *Lawrence et al.* [2011] point out that GPP in the model is biased high, and soils tend to be unrealistically low in moisture compared to observations. Nevertheless, the land model in the **LGM** experiment contains 579 Pg less carbon than **PRE**, which fits well with the generally accepted reconstruction of 300 to 700 PgC drop under glacial conditions [*Hoogakker et al.*, 2016].

If the discussion above made you doubt the model output, fear not: the aim was to make you doubt climate reconstructions altogether. Indeed, it is quite the task to marry four[27] disciplines of science, each with their own methodology and tendencies, to construct a full picture of the complex system that is our Earth. Even within a single discipline, the task of reconstructing the past is difficult: *Wunsch* [2003] argues that fully understanding the modern overturning circulation is already a great challenge, and that reconstructing the overturning patterns of glacial Earth is no different - yet we rely on a significantly smaller data set for the task. Proxy data are associated with large uncertainties and can be biased[28]. With that in mind, I'd like you to consider how remarkable it is that modern fully coupled models can reproduce key features of the glacials as we know them. The pCO_2 levels from ice cores are some of the most reliable records of the past, as they are direct measurements of past atmospheres, rather than a proxy. The model's ability to reproduce these values in fully coupled systems is a promising step on the way of understanding which climatic processes drive the observed changes in pCO_2.

[26] These estimates are based on pCO_2 levels of about 350 ppm, in contrast to the pre-industrial 280 ppm. The connection between the NPP and pCO_2 is complicated [e.g. *Melillo et al.*, 1993], and therefore this particular verification is meant as an approximate rather than direct comparison.

[27] (Physics, chemistry, biology and geology.)

[28] For example, consider export production: drilling sedimentary cores is expensive and cannot be done just anywhere. In order to minimize errors, the drilling sites are chosen with a hope of finding strong signals. Therefore, we are more likely to get data from sites with strong export production.

Review on the feedback pathways

Let us look back on the negative feedback hypotheses and what the model output can tell us about them.

The **(TT)** pathway predicts that after reaching a certain threshold of temperature, a large energy storage (such as the ocean) resists further cooling of the Earth system. In the model, we observe that mean ocean temperatures stop declining at the limit of about 0.6°C, despite reduced radiative forcing. The SATs and SSTs have a reduced rate of declining in **LGM5i** and **LGM10i** (fig. 9). Rather than the deep ocean reaching freezing temperatures, what resists the cooling in the model is the intensified AMOC. In figure 10, we see that cooling of the AABW continues between **LGM0**, **LGM5i0** and **LGM10i0**, but the NADW gets warmer. The SAT map (fig. 11) reveals that while the rest of the world is cooling, a single region in the Northern Atlantic sees an increase in temperature. The Gulf Stream, which is a part of AMOC, transports heat from the tropics into high latitudes in the Atlantic. The strong NADW formation in **LGM10i0** (fig. 20) is most likely responsible for heating up the Northern Atlantic and the deep water formed there, which results in the system resisting cooling.

According to the **(CT)** pathway, the negative limit exists due to reduction in the climate sensitivity to CO_2 forcing as the world becomes colder. This is directly in opposition to previous model studies, which show that the Earth system becomes more sensitive to radiative forcing at low greenhouse gas concentrations [e.g. *Manabe and Bryan Jr.*, 1985; *Huang and Bani Shahabadi*, 2014]. Nevertheless, we do observe that the pCO_2-temperature correlation breaks in the sensitivity experiments, and that the temperature stops responding to lower pCO_2 concentrations. In **LGM10i0**, pCO_2 drops by 34 ppm compared to **LGM0**, while the corresponding SAT decrease is only 0.5°C. *Brady et al.* [2013] run a series of LGM simulations in Community Climate System Model 4[29] in order to investigate the radiative forcing parameters. For their $LGMCO_2$ simulation, in which they set the atmospheric pCO_2 to 185 ppm, they find the effective climate feedback parameter λ_{eff} to be 0.85 $Wm^{-2}\,{}^{\circ}C^{-1}$. Using the parameter, together with radiative forcing due to CO_2 calculation

[29] (Identical to CESM1 in properties relevant for this study.)

based on *Ramaswamy et al.* [2001], the rough estimate for expected drop in temperature between **LGM10i0** and **LGM0** is 1°C. What sets apart the output used in this study to *Manabe and Bryan Jr.* [1985], *Huang and Bani Shahabadi* [2014] and *Brady et al.* [2013] is that the LGM conditions develop with coupled biogeochemistry model. Still, it appears more likely that it is the NH warming that counters the radiative forcing of CO_2 effect, rather than the Earth losing sensitivity to lowering CO_2 at cold temperatures.

The **(TC)** pathway involves a mechanism where the Earth system resists further decrease in CO_2 when it gets very cold. The suggested mechanism involves the sea ice extent in the Southern Ocean.

Jochum et al. [submitted] find that the disequilibrium pump, together with the physical aspects of sea water under the LGM conditions, overwhelmingly dominate the glacial pCO_2 drawdown. The disequilibrium DIC increasing in the LGM conditions are due to the ice extent: the air-sea exchange is suppressed, and the light limitation is increased, so that the existing DIC cannot be converted into organic material. Moreover, the physical changes in the atmospheric flows, ie. strenghtening and poleward shift of the Southern Hemisphere (SH) westerlies, result in a shorter time scale of the deep upwelled water seeing the atmosphere. The soft-tissue pump in **LGM** is weaker than in **PRE** (fig. 17). Although export production is increased, the average water age decreases by 500 years, which results in relatively faster cycling of DIC_{soft} and other nutrients. Therefore, it is primarily the disequilibrium and solubility which contribute to the pCO_2 drawdown.

In the context of this and the results showed in this report, the model shows what G&E predict to some extent. The Southern Ocean and sea ice extending induce the LGM conditions by sequestering carbon in the form of DIC_{dis} and DIC_{sat}, additionally DIC_{soft} when iron fertilization is utilized. However, in the model SO, the capping effect of the ice seems to favor DIC outgassing when ice fraction is over 75%,. We know that although the ice fraction change is relatively small between **LGM10i0** and **LGM0**, the phytoplankton light limitation is sensitive to it (figs. 22 and 23). This could indicate that when ice grows further equator-

ward, it might cover the region where the phytoplankton resides and suppress the DIC uptake.

The **(CC)** pathway contains two different hypotheses, both of which are based on assumptions not implemented in the model. The **(CC^a)** hypothesis suggests that with dropping CO_2 levels, the photosynthesis rates in the Earth's ecosystems are reduced, which then leads to accumulation of CO_2 in the atmosphere. Neither land nor marine photosynthesis is limited by background pCO_2. We do see the land carbon loss in the model (fig. 31), but this is due to colder, dryer environment.

The **(CC^b)** hypothesis suggests that at pCO_2 levels below 180 ppm, the marine diazotrophs die out, which significantly reduces other phytoplankton cultures' access to nitrate. Although the model does not include a pCO_2 limitation for diazotrophs, we still see a significant drop in diazotroph chlorophyll concentration between **LGM5i0** and **LGM10i0** (fig. 24) due to nutrient trapping in the SO. We see that diatoms in high latitudes get more limited by nitrate availability in **LGM10i0** compared to **LGM0** and **PRE** (fig. 45 in the Appendix), but the effects of nutrient trapping and reduction in diazotroph chlorophyll are not possible to decouple.

The nutrient trapping opens up another interesting hypothesis for a series of processes which keep pCO_2 above the 190 ppm threshold. When the Southern Ocean, a HNLC region, is fertilized with iron, the phytoplankton activity increases. This growth has a potential for enhancing carbon uptake from the atmosphere, which is demonstrated in the **LGM5i** and **LGM10i** experiments. However, although **LGM10i** has a higher DIC_{soft} content in the deep ocean, **LGM5i** has a higher export production in the euphotic zone (fig. 28). This is because the nutrient supplier for the surface waters of the Atlantic is the upwelling zone around Antarctica, which runs dry when the phytoplankton activity increases in the region. This opens up a discussion on whether this effect has a cap: if we fertilize the ocean with progressively more iron, is the Atlantic eventually drained of nutrients, which prevents any biological activity in these waters, resulting in a net outgassing of DIC? Or does the phytoplankton eventually become oversaturated with iron, and the Atlantic never reaches the state in which it tips the global DIC flux into outgassing?

Gaps which need filling

The extent of the material covered in this study required a certain level of prioritizing between the topics. The work I have done on the LGM output is not exhaustive of what could be found among the hundreds of variables of CESM1. A continuation of exploring the **(TT)** and the **(CT)** pathways could be an in-depth analysis of energy fluxes at TOA, the albedo feedbacks and the wind patterns. These were down-prioritized due to likelihood that the changes would be too small to draw conclusions, especially considering the extent of the influence of D-O oscillations on the stadial and interstadial results. There is a number of puzzling results which were not addressed in this study, for example the shut down of SOMOC in the **LGM10i0** interstadial, and lack thereof in **LGM5i0**, while both of them exhibiting changes in AMOC (fig. 20). **LGMd** was seldom mentioned and the effects of enhanced mixing were only superficially analyzed.

The further analysis of the **(TC)** and **(CC)** pathways would require additional model runs. Quantifying how much ice extend would be needed for the SO to become dominated by DIC outgassing and what the Earth system would look like in such setup could help assess the plausibility of the **(TC)** pathway. Testing the **(CC)** hypotheses would require a more involved model alterations: already in the current setup, there are issues with representing realistic diazotroph limitations [*Moore et al.*, 2004]. Introducing a pCO_2 limitation adds complexity, while the effect lacks constraints, as the limit has only ever been observed in a lab [*Hutchins et al.*, 2013]. Likewise, introducing pCO_2 limitation to the model would be difficult to constrain, as the effects of changing carbon dioxide concentrations and temperature are not always multiplicative [*Wang et al.*, 2012]. Therefore, using models of lower complexity and observations to constrain the effects of background pCO_2 concentrations is in order before the fully coupled models can tackle the issue.

Meanwhile, getting rid of the ventilation bias in the BGC component of CESM1 could in principle improve modeled the DIC_{soft} concentration estimates. The Redfield ratios in the model are kept fixed both in the land and marine ecosystems, as it is known that the ratios stay constant in global averages. However, in real

ecosystems, plants and phytoplankton can adapt their C/N/P ratios if they are N- or P-limited [e.g. *Sarmiento and Gruber*, 2006]. *Ödalen et al.* [2018] present results from their simulations in cGENIE model which indicate that allowing simulated phytoplankton groups to adapt their Redfield ratios to low-nutrient conditions results in up to 15 ppm more CO_2 drawdown in the LGM conditions. This could be an interesting effect to investigate in a model of finer resolution such as CESM1.

The effect of nutrient trapping could be further explored, both with the existing model output and more modeling work. Enhancing dust fluxes regionally rather than uniformly to match the reconstructions cited in *Lambert et al.* [2015] could potentially remove the bias outlined by *Möllney* [2020]. Moreover, fertilizing the SO with 20 to 30 times higher iron fluxes could test whether the phytoplankton eventually becomes oversaturated with the micro-nutrient, or whether the nutrient trapping effect intensifies. It would certainly be interesting to see the pCO_2 response to the Earth system where the nitrate and phosphate depleted regions in the ocean dominate the iron fertilization in the SO.

Light at the end of the tunnel

What did we learn about the pCO_2-temperature correlation problem? To cite *Galbraith and Skinner* [2020], *it's complicated*. The complexity of the Earth system makes it exceedingly difficult to investigate this seemingly trivial problem. Although there are many unknowns, this study finds the following:

- The CESM1 model with the setup outlined in the chapter *Digital twin of Earth* does not resist lowering of pCO_2 beyond the 190 ppm threshold; it does, however, resist cooling when the mean ocean temperatures reach 0.6°C;
- The negative feedback pathway **(CC)** cannot be tested by this model, as the necessary limitations are not implemented;
- The model shows evidence for the **(TT)** and the **(CT)** pathways;
- The **(TC)** pathway could potentially play a role if the sea ice grew further in the SO; with the presented setup, there is no evidence for it;
- Nutrient trapping develops in the model, where the marine productivity is reduced in the Indian and Atlantic basins due to increased phytoplankton activity in the Southern Ocean; there is evidence of weakened global export production at high rates of iron fertilization, which could imply that the reduced productivity in the NH and low latitudes of SH could potentially outweigh the pCO_2 drawdown in the SO.

While a wide range of uncertainties exists, the models are able to reproduce the magnitudes of the glacial pCO_2 drawdowns and corresponding temperatures. It is exactly the number and combination of different processes which can shift the Earth system into that state that poses difficulties. The new ways of

thinking about the pCO_2-temperature correlation problem, such as G&E's negative feedback hypothesis, allow us to find fresh perspectives on how to pinpoint the chain of events that couples these two variables so closely. Meanwhile, we can be motivated to keep looking by Milankovitch's ambition to grasp the entire universe and spread light into its farthest corners.

Bibliography

Abe-Ouchi, A., F. Saito, K. Kawamura, M. E. Raymo, J. Okuno, K. Takahashi, and H. Blatter, Insolation-driven 100,000-year glacial cycles and hysteresis of ice-sheet volume, *Nature*, *500*(7461), 190–3, DOI: 10.1038/nature12374, 2013.

Annan, J., and J. C. Hargreaves, A new global reconstruction of temperature changes at the last glacial maximum, *Climate of the Past*, *9*(1), 367–376, DOI: 10.5194/cp-9-367-2013, 2013.

Beer, J., Sun and climate, *SPATIUM*, (8), 2–19, 2001.

Bereiter, B., S. Shackleton, D. Baggenstos, K. Kawamura, and J. Severinghaus, Mean global ocean temperatures during the last glacial transition, *Nature*, *553*(7686), 39–44, DOI: 10.1038/nature25152, 2018.

Berger, A., Milankovitch, the father of paleoclimate modelling, *Climate of the Past Discussions*, *2021*, 1–10, 2021.

Bergman, B., G. Sandh, S. Lin, J. Larsson, and E. J. Carpenter, Trichodesmium–a widespread marine cyanobacterium with unusual nitrogen fixation properties, *FEMS microbiology reviews*, *37*(3), 286–302, DOI: 10.1111/j.1574-6976.2012.00352.x, 2013.

Bernardello, R., I. Marinov, J. B. Palter, J. L. Sarmiento, E. D. Galbraith, and R. D. Slater, Response of the ocean natural carbon storage to projected twenty-first-century climate change, *Journal of Climate*, *27*(5), 2033–2053, DOI: 10.1175/JCLI-D-13-00343.1, 2014.

Brady, E. C., B. L. Otto-Bliesner, J. E. Kay, and N. Rosenbloom, Sensitivity to glacial forcing in the ccsm4, *Journal of Climate*, *26*(6), 1901–1925, DOI: 10.1175/JCLI-D-11-00416.1, 2013.

Bryan, K., and L. Lewis, A water mass model of the world ocean, *Journal of Geophysical Research: Oceans*, *84*(C5), 2503–2517, DOI: 10.1029/JC084iC05p02503, 1979.

Cartapanis, O., D. Bianchi, S. L. Jaccard, and E. D. Galbraith, Global pulses of organic carbon burial in deep-sea sediments during glacial maxima, *Nature communications*, *7*(1), 1–7, DOI: 10.1038/ncomms10796, 2016.

Chalk, T. B., et al., Causes of ice age intensification across the mid-pleistocene transition, *Proceedings of the National Academy of Sciences of the United States of America*, *114*(50), 13,114–13,119, DOI: 10.1073/pnas.1702143114, 2017.

Ciais, P., et al., Large inert carbon pool in the terrestrial biosphere during the last glacial maximum, *Nature Geoscience*, *5*(1), 74–79, DOI: 10.1038/ngeo1324, 2012.

Ciais, P., et al., *Carbon and Other Biogeochemical Cycles. In: Climate Change 2013: The Physical Science Basis. Contribution of Working Group I to the Fifth Assessment Report of the Intergovernmental Panel on Climate Change*, chap. 6, p. 471, Cambridge University Press, 2013.

Danabasoglu, G., W. G. Large, and B. P. Briegleb, Climate impacts of parameterized nordic sea overflows, *Journal of Geophysical Research: Oceans*, *115*(C11), DOI: 10.1029/2010JC006243, 2010.

Denton, G., R. Anderson, J. Toggweiler, R. Edwards, J. Schaefer, and A. Putnam, The last glacial termination, *Science*, *328*, 1652 – 1656, DOI: 10.1126/science.1184119, 2010.

Du, J., B. A. Haley, and A. C. Mix, Evolution of the global overturning circulation since the last glacial maximum based on marine authigenic neodymium isotopes, *Quaternary Science Reviews*, *241*, 106,396, DOI: 10.1016/j.quascirev.2020.106396, 2020.

Eggleston, S., and E. D. Galbraith, The devil's in the disequilibrium: multi-component analysis of dissolved carbon and oxygen changes under a broad range of forcings in a general circulation model, *Biogeosciences*, *15*, 3761–3777, DOI: 10.5194/bg-15-3761-2018, 2018.

Forseth, I. N., The ecology of photosynthetic pathways, *Nature Education Knowledge*, *3*(10), 4, 2010.

Galbraith, E., and S. Eggleston, A lower limit to atmospheric co2 concentrations over the past 800,000 years, *Nature Geoscience*, *10*, 295–298, DOI: 10.1038/ngeo2914, 2017.

Galbraith, E. D., and L. C. Skinner, The biological pump during the last glacial maximum, *Annual review of marine science*, *12*, 559–586, DOI: 10.1146/annurev-marine-010419-010906, 2020.

Goosse, H., *Climate System Dynamics and Modelling*, Cambridge University Press, 2015.

Gough, C. M., Terrestrial primary production: Fuel for life, *Nature Education Knowledge*, *3*(10), 28, 2011.

Gupta, M., M. J. Follows, and J. M. Lauderdale, The effect of antarctic sea ice on southern ocean carbon outgassing: Capping versus light attenuation, *Global Biogeochemical Cycles*, *34*(8), e2019GB006,489, DOI: 10.1126/10.1029/2019GB006489, 2020.

Hain, M., D. Sigman, and G. Haug, 8.18–the biological pump in the past, *Reference Module in Earth Systems and Environmental Sciences, Treatise on Geochemistry (Second Edition), The Oceans and Marine Geochemistry*, *8*, 485–517, DOI: 10.1016/B978-0-08-095975-7.00618-5, 2014.

Hoogakker, B., et al., Terrestrial biosphere changes over the last 120 kyr, *Climate of the Past*, *12*, 51–73, DOI: 10.5194/cp-12-51-2016, 2016.

Huang, Y., and M. Bani Shahabadi, Why logarithmic? a note on the dependence of radiative forcing on gas concentration, *Journal of Geophysical Research: Atmospheres*, *119*(24), 13,683–13,689, DOI: 10.1002/2014JD022466, 2014.

Hurrell, J. W., et al., The community earth system model: a framework for collaborative research, *Bulletin of the American Meteorological Society*, *94*(9), 1339–1360, DOI: 10.1175/BAMS-D-12-00121.1, 2013.

Hutchins, D. A., F. Fu, Y. Zhang, M. E. Warner, Y. Feng, K. Portune, P. W. Bernhardt, and M. R. Mulholland, Co2 control of trichodesmium n2 fixation, photosynthesis, growth rates, and

elemental ratios: Implications for past, present, and future ocean biogeochemistry, *Limnology and Oceanography*, *52*(4), 1293–1304, DOI: 10.4319/lo.2007.52.4.1293, 2007.

Hutchins, D. A., F.-X. Fu, E. A. Webb, N. Walworth, and A. Tagliabue, Taxon-specific response of marine nitrogen fixers to elevated carbon dioxide concentrations, *Nature Geoscience*, *6*(9), 790–795, DOI: 10.1038/ngeo1858, 2013.

Imbrie, J., et al., On the structure and origin of major glaciation cycles 1. linear responses to milankovitch forcing, *Paleoceanography*, *7*(6), 701–738, DOI: 10.1029/92PA02253, 1992.

Ito, T., M. Follows, and E. Boyle, Is aou a good measure of respiration in the oceans?, *Geophysical Research Letters*, *31*(17), DOI: 10.1029/2004GL020900, 2004.

Jickells, T., et al., Global iron connections between desert dust, ocean biogeochemistry, and climate, *science*, *308*(5718), 67–71, DOI: 10.1126/science.1105959, 2005.

Jochum, M., A. Jahn, S. Peacock, D. A. Bailey, J. T. Fasullo, J. Kay, S. Levis, and B. Otto-Bliesner, True to milankovitch: Glacial inception in the new community climate system model, *Journal of Climate*, *27*(7), 2226–2239, DOI: 10.1175/JCLI-D-11-00044.1, 2012.

Jochum, M., G. Vettoretti, R. Nuterman, and Z. Chase, Carbon pools in a last glacial maximum integration of a fully coupled earth system model [submitted for publication], submitted.

Khatiwala, S., A. Schmittner, and J. Muglia, Air-sea disequilibrium enhances ocean carbon storage during glacial periods, *Science advances*, *5*(6), eaaw4981, DOI: 10.1126/sciadv.aaw4981, 2019.

Kohfeld, K. E., and Z. Chase, Temporal evolution of mechanisms controlling ocean carbon uptake during the last glacial cycle, *Earth and Planetary Science Letters*, *472*, 206–215, DOI: 10.1126/science.aao6379, 2017.

Kohfeld, K. E., C. Le Quéré, S. P. Harrison, and R. F. Anderson, Role of marine biology in glacial-interglacial co2 cycles, *Science*, *308*(5718), 74–78, DOI: 10.1126/science.1105375, 2005.

Lambert, F., A. Tagliabue, G. Shaffer, F. Lamy, G. Winckler, L. Farias, L. Gallardo, and R. De Pol-Holz, Dust fluxes and iron fertilization in holocene and last glacial maximum climates, *Geophysical Research Letters*, *42*(14), 6014–6023, DOI: 10.1002/2015GL064250, 2015.

Lawrence, D. M., et al., Parameterization improvements and functional and structural advances in version 4 of the community land model, *Journal of Advances in Modeling Earth Systems*, *3*(1), DOI: 10.1029/2011MS00045, 2011.

Lawrence, P. J., and T. N. Chase, Representing a new modis consistent land surface in the community land model (clm 3.0), *Journal of Geophysical Research: Biogeosciences*, *112*(G1), DOI: 10.1029/2006JG000168, 2007.

Lindsay, K., et al., Preindustrial-control and twentieth-century carbon cycle experiments with the earth system model cesm1(bgc), *Journal of Climate*, *27*, 8981–9005, DOI: 10.1175/JCLI-D-12-00565.1, 2014.

Lynch-Stieglitz, J., et al., Atlantic meridional overturning circulation during the last glacial maximum, *science*, *316*(5821), 66–69, DOI: 10.1126/science.1137127, 2007.

Manabe, S., and K. Bryan Jr., Co2-induced change in a coupled ocean-atmosphere model and its paleoclimatic implications, *Journal of Geophysical Research: Oceans*, *90*(C6), 11,689–11,707, DOI: 10.1029/JC090iC06p11689, 1985.

Martin, J. H., Glacial - interglacial co2 change: the iron hypothesis, *Paleoceanography*, *5*(1), 1–13, DOI: 10.1029/PA005i001p00001, 1990.

Melillo, J. M., A. D. McGuire, D. W. Kicklighter, B. Moore, C. J. Vorosmarty, and A. L. Schloss, Global climate change and terrestrial net primary production, *Nature*, *363*(6426), 234–240, DOI: 10.1038/363234a0, 1993.

Moore, J. K., S. C. Doney, and K. Lindsay, Upper ocean ecosystem dynamics and iron cycling in a global three-dimensional model, *Global Biogeochemical Cycles*, *18*(4), DOI: 10.1029/2004GB002220, 2004.

Moore, J. K., et al., Sustained climate warming drives declining marine biological productivity, *Science*, *359*(6380), 1139–1143, DOI: 10.1126/science.aao6379, 2018.

Möllney, L., Patterns of dust-borne iron fertilization at the last glacial maximum, Master's thesis, University of Hamburg and Max-Planck-Institute for Meteorology and Physics of Ice, Climate and Earth, Niels Bohr Institute, Copenhagen University, 2020.

Neftel, A., H. Oeschger, J. Schwander, B. Stauffer, and R. Zumbrunn, Ice core sample measurements give atmospheric co 2 content during the past 40,000 yr, *Nature*, *295*(5846), 220–223, DOI: 10.1038/295220a0, 1982.

Ödalen, M., J. Nycander, A. Ridgwell, K. Oliver, and J. Nilsson, Non-Redfield composition of organic production and its effect on ocean carbon storage in glacial model simulations, in *EGU General Assembly Conference Abstracts*, EGU General Assembly Conference Abstracts, p. 13010, 2018.

Peacock, S., E. Lane, and J. M. Restrepo, A possible sequence of events for the generalized glacial-interglacial cycle, *Global Biogeochemical Cycles*, *20*(2), DOI: 10.1029/2005GB002448, 2006.

Ramaswamy, V., O. Boucher, J. Haigh, D. Hauglustaine, J. Haywood, G. Myhre, T. Nakajima, G. Shi, and S. Solomon, Ipcc third assessment report, 350 pp, 2001.

Raymo, M. E., and K. H. Nisancioglu, The 41 kyr world: Milankovitch's other unsolved mystery, *Paleoceanography*, *18*(1), DOI: 10.1029/2002PA000791, 2003.

Sarmiento, J. L., and N. Gruber, *Ocean Biogeochemical Dynamics*, Princeton University Press, 2006.

Schmitt, J., et al., Carbon isotope constraints on the deglacial co2 rise from ice cores, *Science (New York, N.Y.)*, *336*, 711–4, DOI: 10.1126/science.1217161, 2012.

Shields, C. A., D. A. Bailey, G. Danabasoglu, M. Jochum, J. T. Kiehl, S. Levis, and S. Park, The low-resolution ccsm4, *Journal of Climate*, *25*(12), 3993–4014, DOI: 10.1175/JCLI-D-11-00044.1, 2012.

Stephens, B. B., and R. F. Keeling, The influence of antarctic sea ice on glacial–interglacial co 2 variations, *Nature*, *404*(6774), 171–174, DOI: 10.1038/35004556, 2000.

Talley, L. D., Closure of the global overturning circulation through the indian, pacific, and southern oceans: Schematics and transports, *Oceanography*, *26*(1), 80–97, DOI: 10.5670/oceanog.2013.07, 2013.

Thornton, P. E., et al., Modeling and measuring the effects of disturbance history and climate on carbon and water budgets in evergreen needleleaf forests, *Agricultural and forest meteorology*, *113*(1-4), 185–222, DOI: 10.1016/S0168-1923(02)00108-9, 2002.

Toggweiler, J. R., J. L. Russell, and S. R. Carson, Midlatitude westerlies, atmospheric co2, and climate change during the ice ages, *Paleoceanography*, *21*(2), DOI: 10.1029/2005PA001154, 2006.

Vettoretti, G., and W. R. Peltier, Interhemispheric air temperature phase relationships in the nonlinear dansgaard-oeschger oscillation, *Geophysical Research Letters*, *42*(4), 1180–1189, DOI: 10.1002/2014GL062898, 2015.

Wang, D., S. A. Heckathorn, X. Wang, and S. M. Philpott, A meta-analysis of plant physiological and growth responses to temperature and elevated co 2, *Oecologia*, *169*(1), 1–13, DOI: 10.1007/s00442-011-2172-0, 2012.

Williams, R. G., and M. J. Follows, *Ocean Dynamics and the Carbon Cycle*, Cambridge University Press, 2011.

Wunsch, C., Determining paleoceanographic circulations, with emphasis on the last glacial maximum, *Quaternary Science Reviews*, *22*(2-4), 371–385, DOI: 10.1016/S0277-3791(02)00177-4, 2003.

Appendix

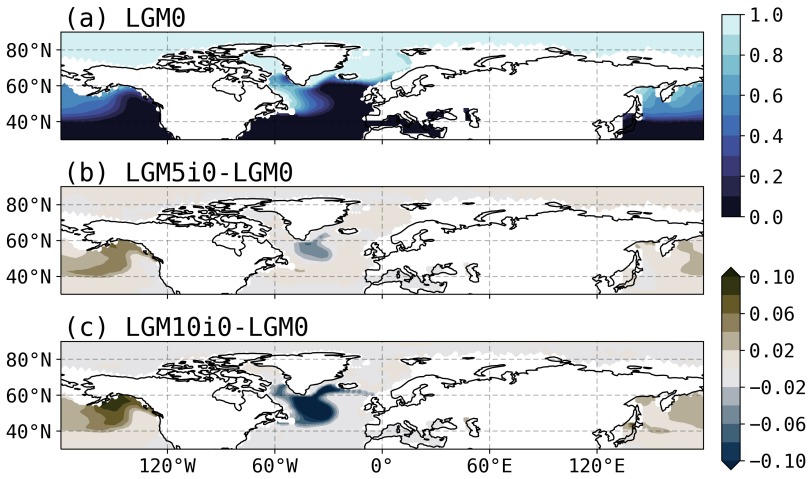

Figure 36: Sea ice fraction in (a) **LGM0**, (b) **LGM5i0-LGM0** and (c) **LGM10i0-LGM0** in high latitudes of the Northern Hemisphere. The "hot pocket" in the Northern Atlantic causes the sea ice to retreat dramatically in the **LGM10i0** interstadial. The sea ice in the Northern Pacific Ocean continues to grow as SAT drops in the iron fertilization experiments.

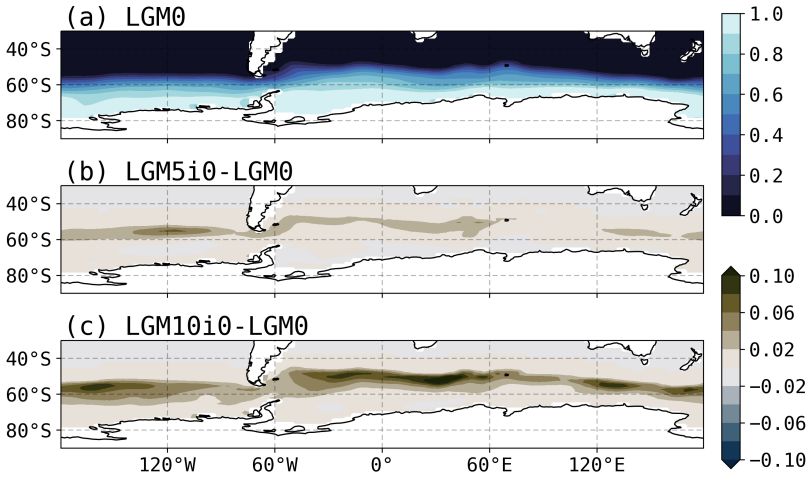

Figure 37: Sea ice fraction in (a) **LGM0**, (b) **LGM5i0-LGM0** and (c) **LGM10i0-LGM0** in the SO.

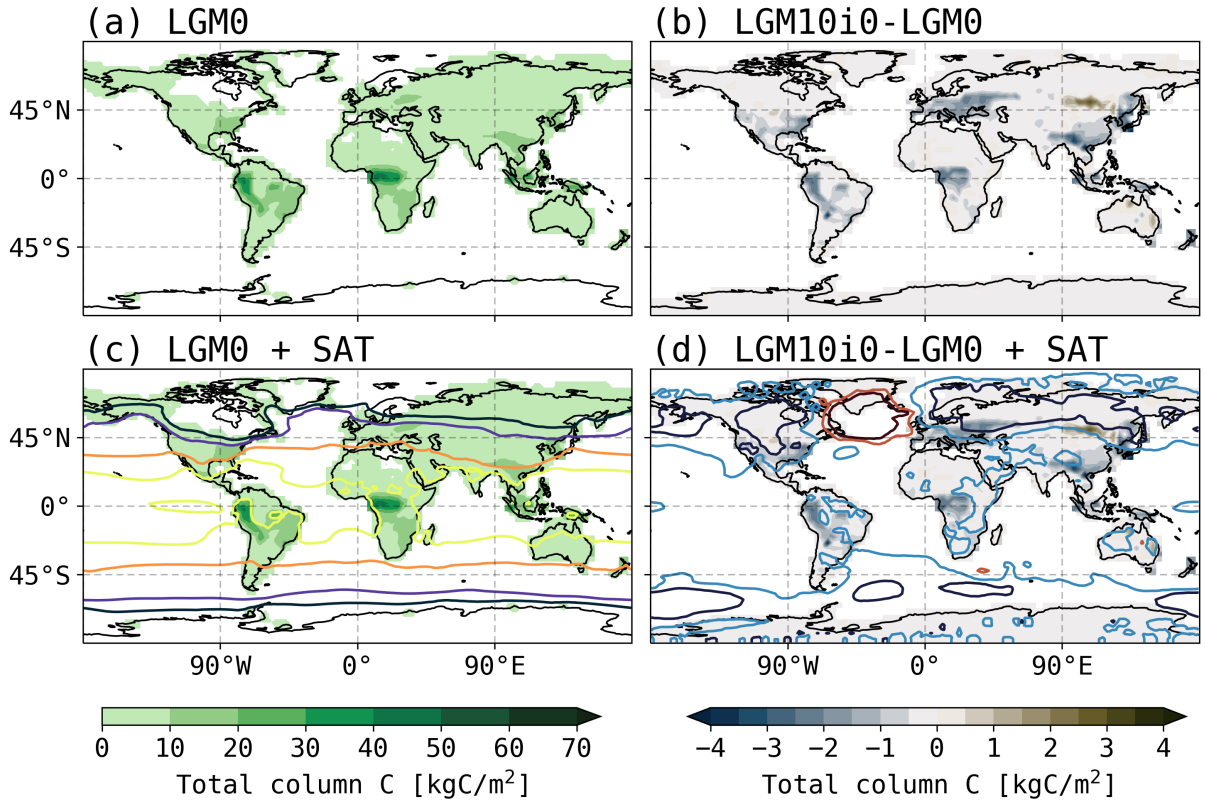

Figure 38: Total column carbon in (a) **LGM0** and (b) **LGM10i0-LGM0**. In (c) and (d), the two maps are overlaid with contours for SAT. In (c) the contours show the surface temperatures in **LGM0**: 20°C (yellow), 10°C (orange), -10°C (purple) and -20°C (dark blue). In (d), the contours show the difference in surface temperatures between **LGM10i0** and **LGM0**: 1°C (dark red), 0.5°C (red), -0.5°C (blue) and -1°C (dark blue).

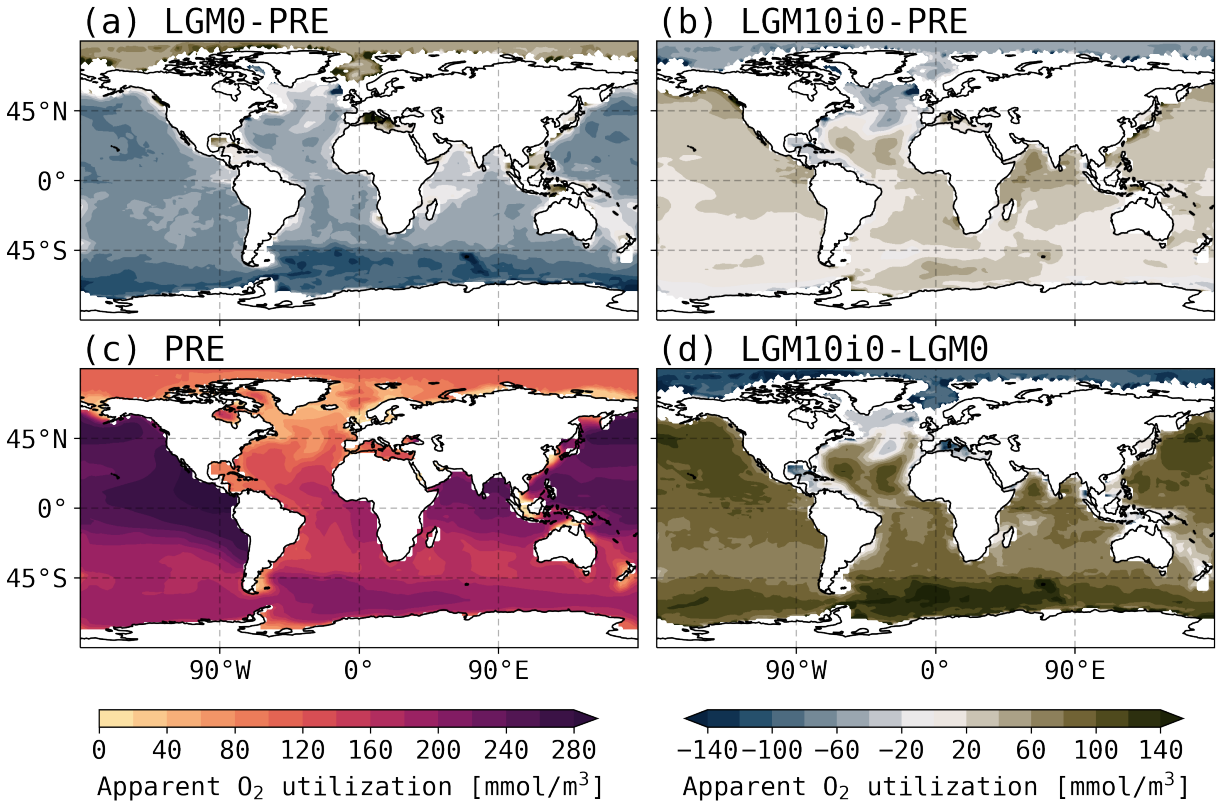

Figure 39: The depth average of AOU, which is proportional to DIC_{soft}, in: (a) **LGM0-PRE**; (b) **LGM10i0-PRE**; (c) **PRE** and (d) **LGM10i0-LGM0**.

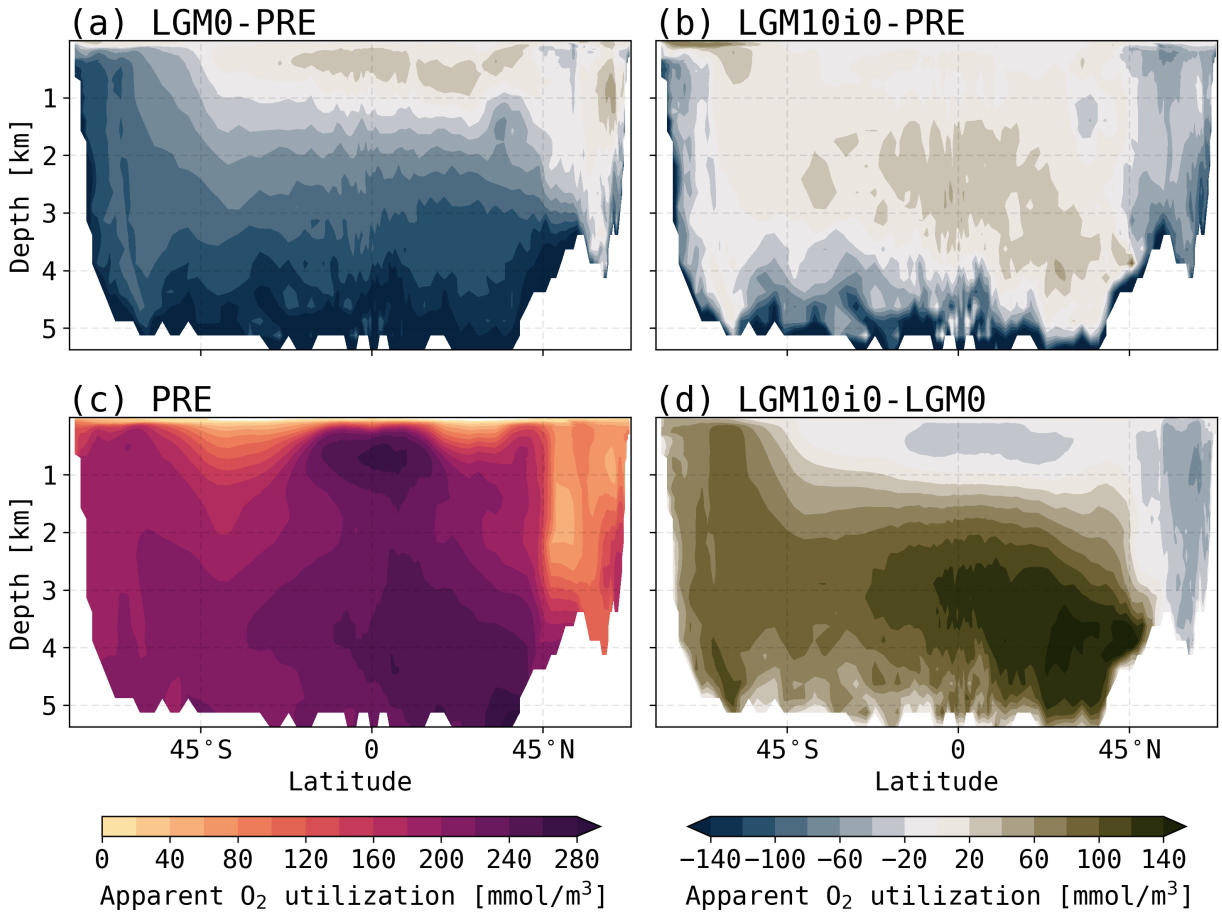

Figure 40: The zonal average of AOU, which is proportional to DIC_{soft}, in: (a) **LGM0-PRE**; (b) **LGM10i0-PRE**; (c) **PRE** and (d) **LGM10i0-LGM0**.

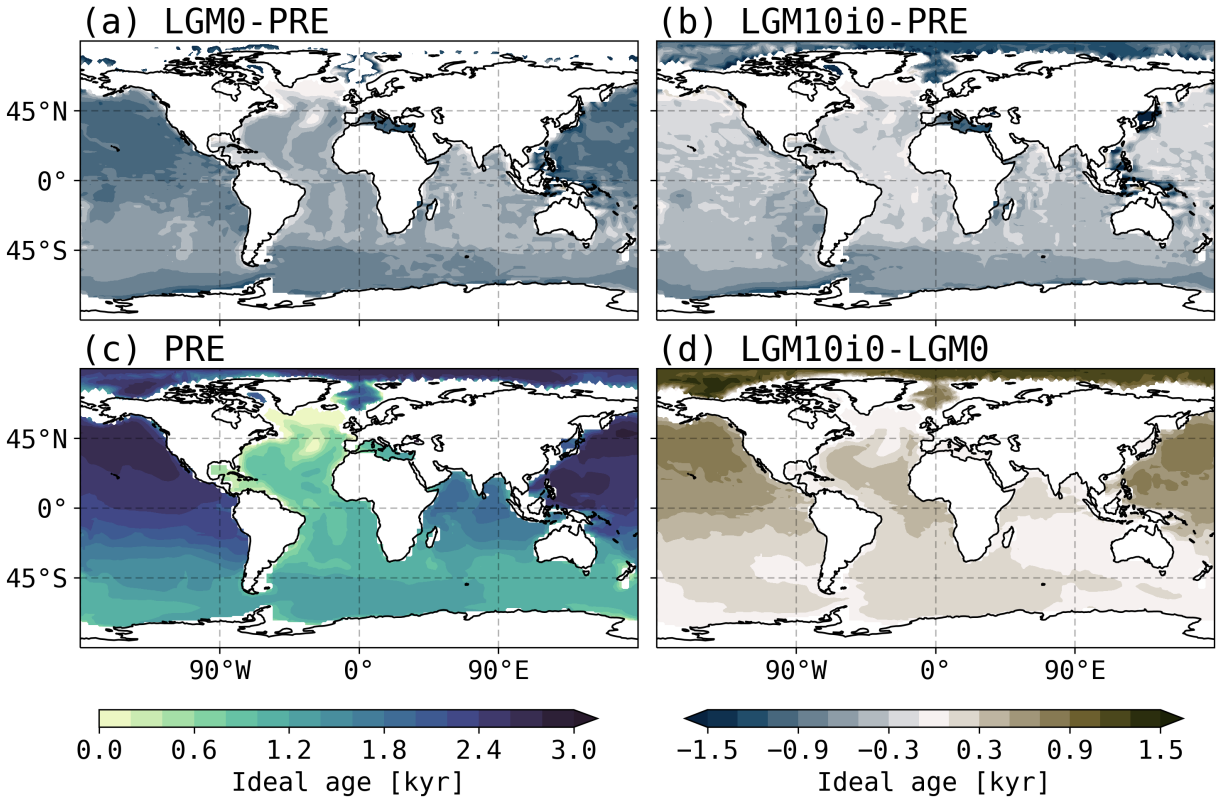

Figure 41: The mean ideal age for the water column below 1000 meters in (a) **LGM0-PRE**; (b) **LGM10i0-PRE**; (c) **PRE** and (d) **LGM10i0-LGM0**.

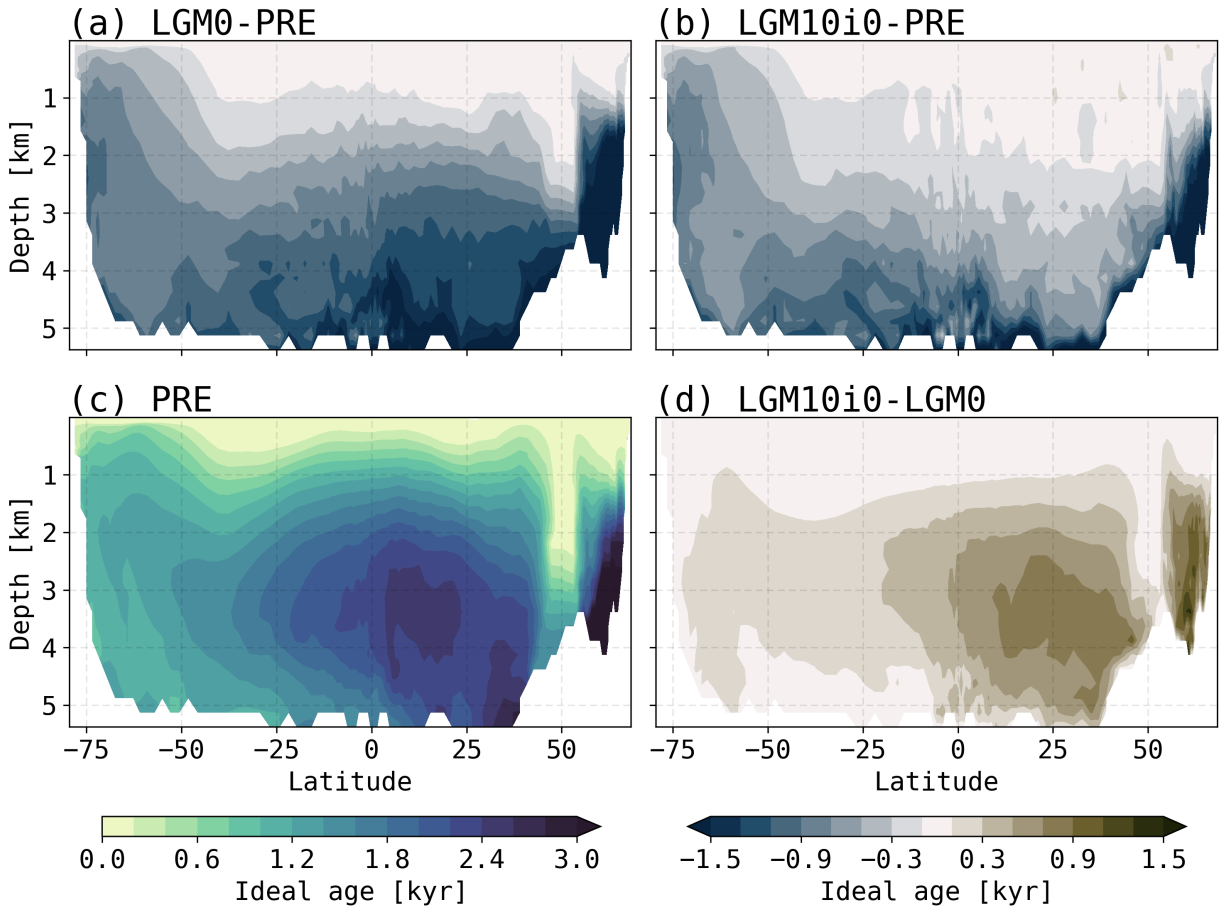

Figure 42: The zonal mean ideal age in: (a) **LGM0-PRE**; (b) **LGM10i0-PRE**; (c) **PRE** and (d) **LGM10i0-LGM0**.

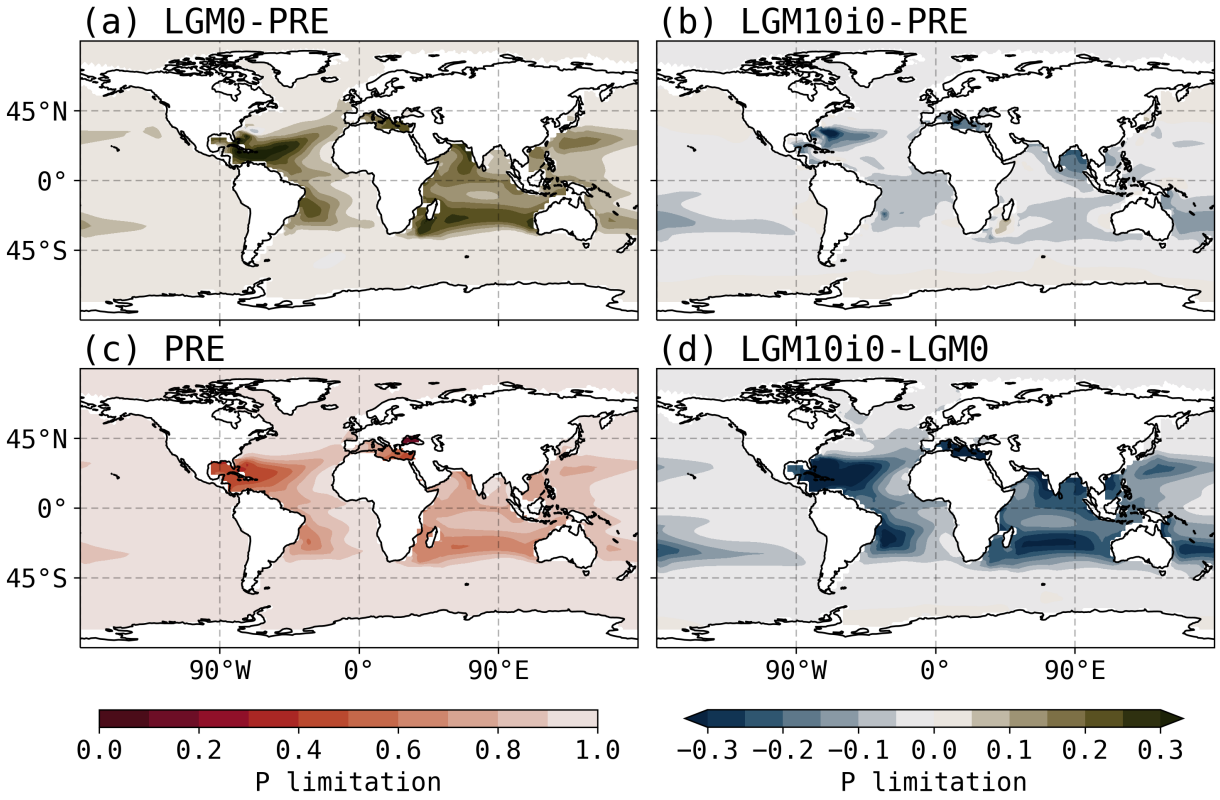

Figure 43: The euphotic zone (top 150 meters) mean phosphate limitation for diazotrophs in the global ocean in: (a) **LGM0-PRE**; (b) **LGM10i0-PRE**; (c) **PRE** and (d) **LGM10i0-LGM0**. Value of 1 indicates no limitation to growth in the given region, while 0 means that no diazotrophs can grow due to unavailability of the nutrient.

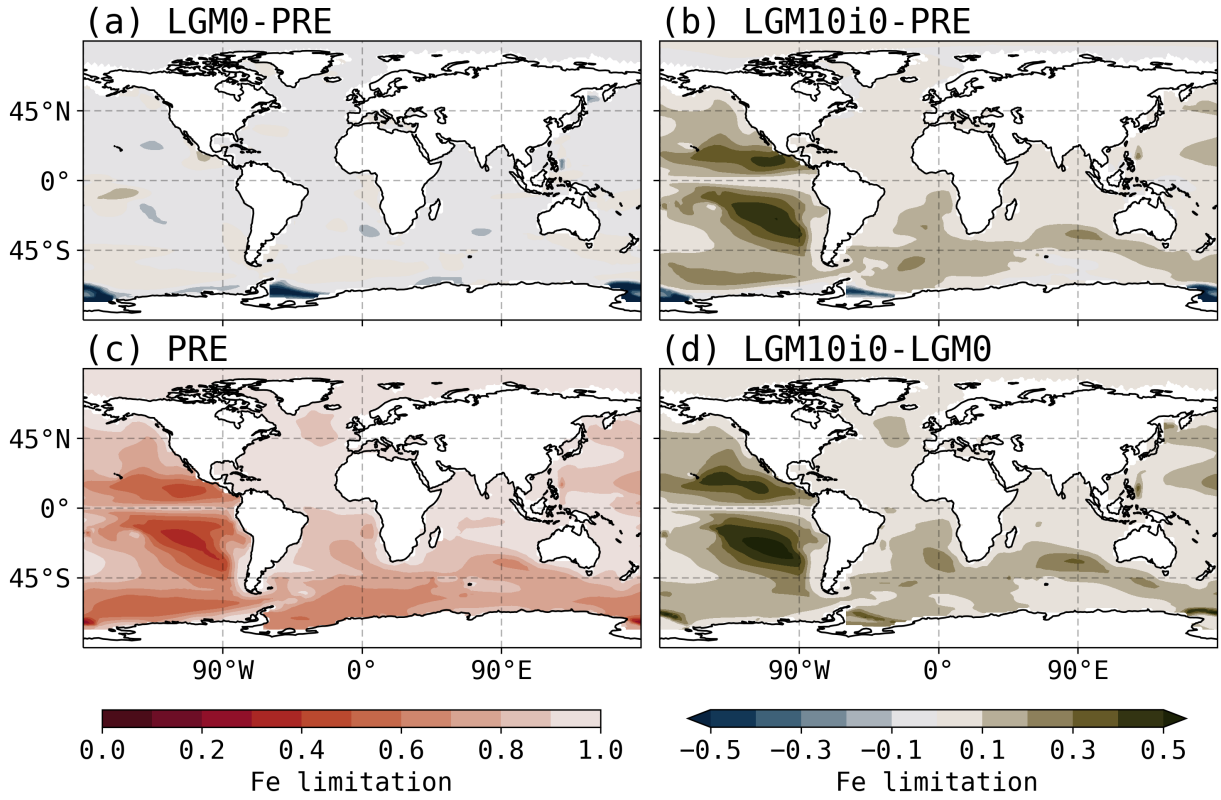

Figure 44: The euphotic zone (top 150 meters) mean iron limitation for diazotrophs in the global ocean in: (a) **LGM0-PRE**; (b) **LGM10i0-PRE**; (c) **PRE** and (d) **LGM10i0-LGM0**.

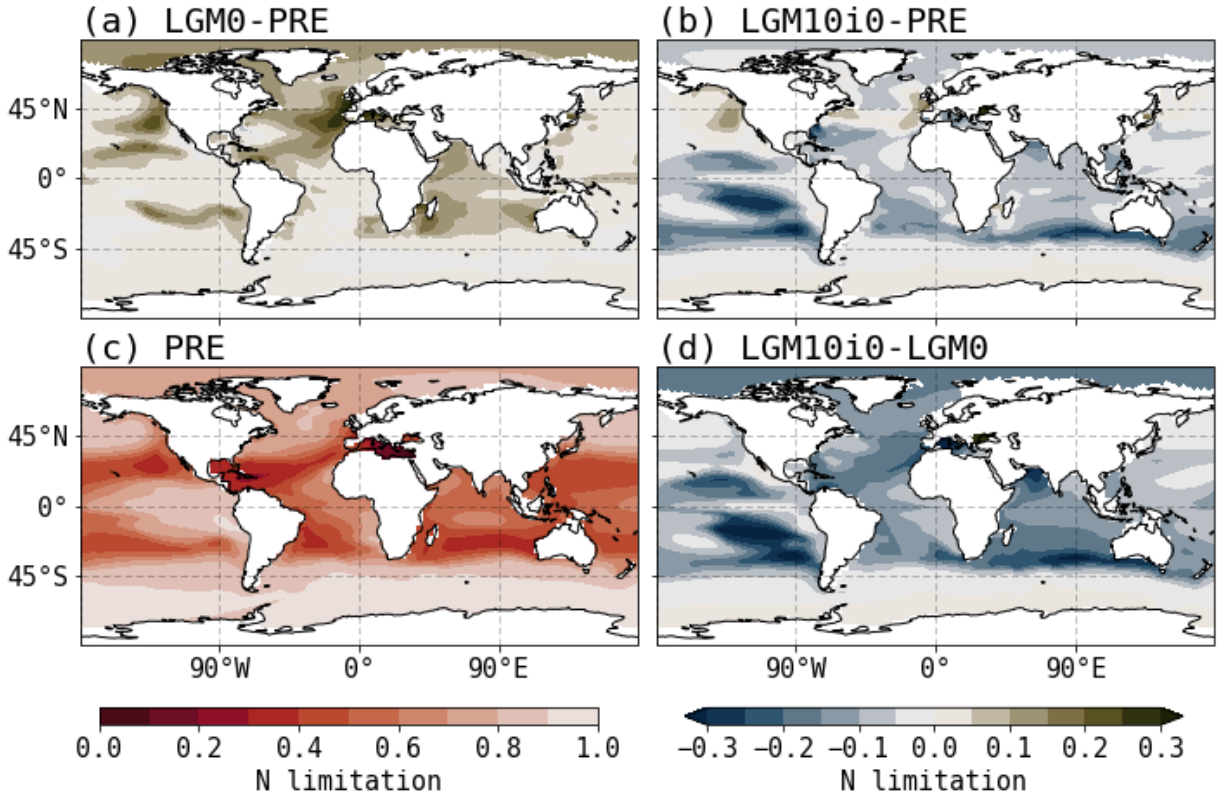

Figure 45: The euphotic zone (top 150 meters) mean nitrate limitation for diatoms in the global ocean in: (a) **LGM0-PRE**; (b) **LGM10i0-PRE**; (c) **PRE** and (d) **LGM10i0-LGM0**.

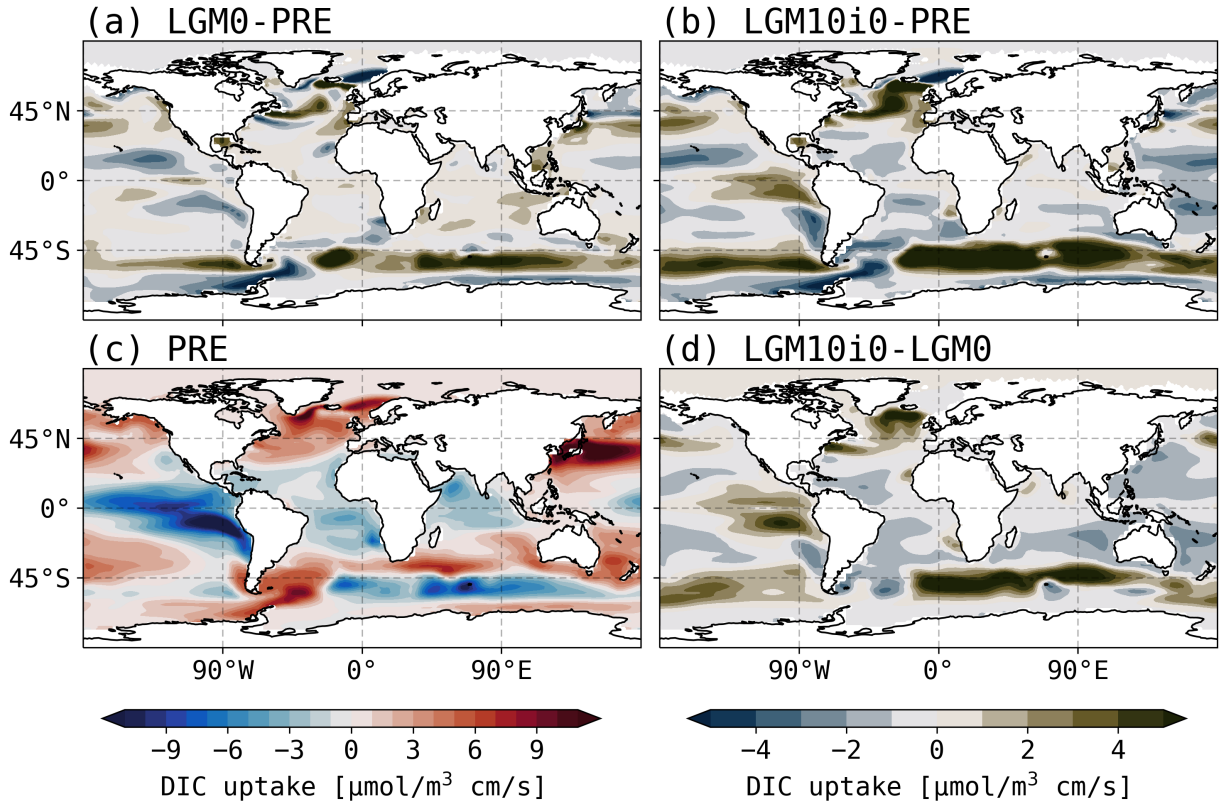

Figure 46: The global patterns of DIC flux between the ocean and the atmosphere in: (a) **LGM0-PRE**; (b) **LGM10i0-PRE**; (c) **PRE** and (d) **LGM10i0-LGM0**. In **PRE**, red shows ocean uptake, and blue shows ocean outgassing